iScience

CellPress
OPEN ACCESS

Article

Creatine kinase brain-type regulates BCAR1 phosphorylation to facilitate DNA damage repair

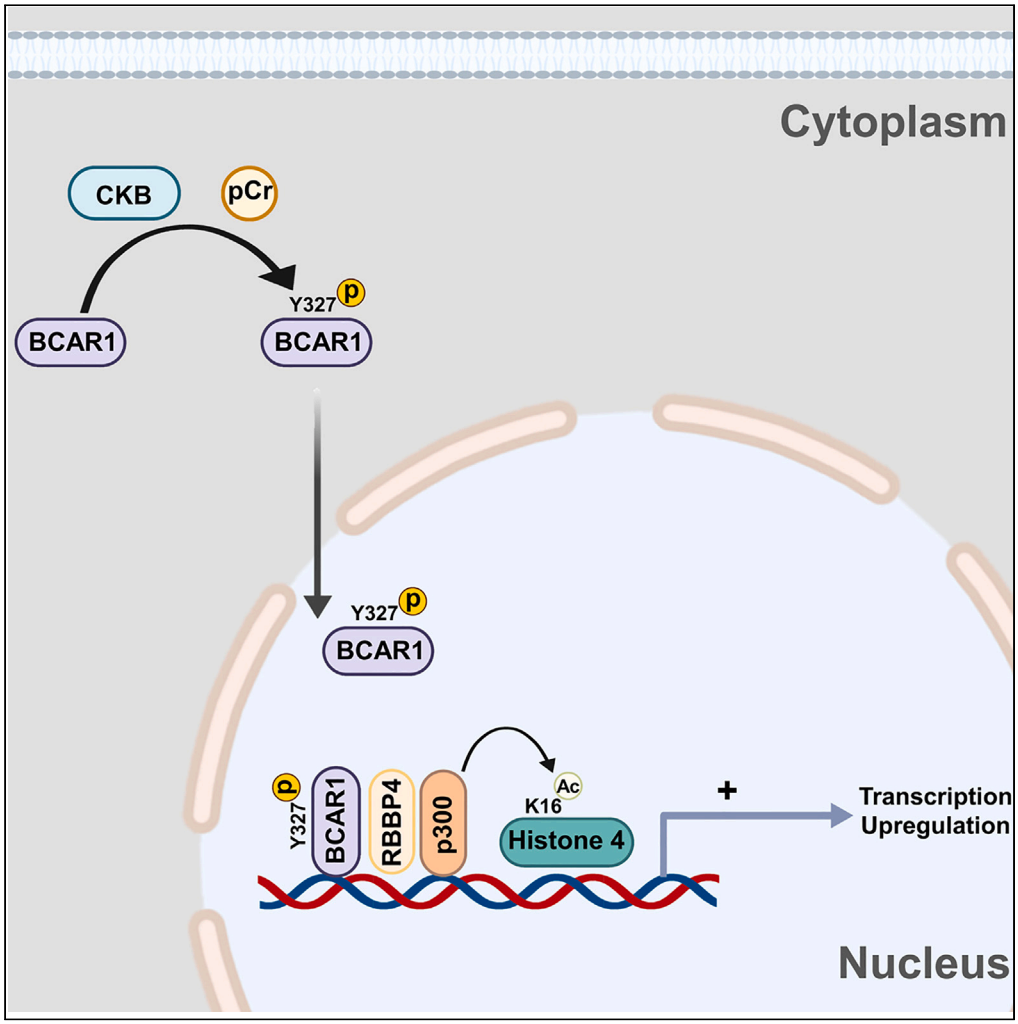

Bo Yang, Wentao Zhang, Le Sun, Bin Lu, Changsong Yin, Yaoyang Zhang, Hong Jiang

hongjiang@sioc.ac.cn

Highlights

CKB functions as a protein kinase to phosphorylate BCAR1 at Y327

BCAR1 pY327 enhances the binding of BCAR1 with RBBP4

BCAR1-RBBP4 complex binds RAD51 promoter region to promote DNA damage repair

Yang et al., iScience 26, 106684
May 19, 2023
https://doi.org/10.1016/j.isci.2023.106684

iScience

CellPress
OPEN ACCESS

Article

Creatine kinase brain-type regulates BCAR1 phosphorylation to facilitate DNA damage repair

Bo Yang,[1,2,4] Wentao Zhang,[1,3,4] Le Sun,[1,3] Bin Lu,[1] Changsong Yin,[1] Yaoyang Zhang,[1,3] and Hong Jiang[1,3,5,*]

SUMMARY

Creatine kinase (CK) is an essential metabolic enzyme mediating creatine/phosphocreatine interconversion and shuttle to replenish ATP for energy needs. Ablation of CK causes a deficiency in energy supply that eventually results in reduced muscle burst activity and neurological disorders in mice. Besides the well-established role of CK in energy-buffering, the mechanism underlying the non-metabolic function of CK is poorly understood. Here we demonstrate that creatine kinase brain-type (CKB) may function as a protein kinase to regulate BCAR1 Y327 phosphorylation that enhances the association between BCAR1 and RBBP4. Then the complex of BCAR1 and RPPB4 binds to the promoter region of DNA damage repair gene *RAD51* and activates its transcription by modulating histone H4K16 acetylation to ultimately promote DNA damage repair. These findings reveal the possible role of CKB independently of its metabolic function and depict the potential pathway of CKB-BCAR1-RBBP4 operating in DNA damage repair.

INTRODUCTION

As a metabolic enzyme, creatine kinase (CK) catalyzes the reversible reaction between creatine (Cr)/ATP and phosphocreatine (PCr)/ADP to regenerate ATP for energy demands or restore PCr as the energy reservoir.[1,2] Found in diverse tissues and cell types in vertebrate animals, CK is expressed in four isoforms, including two cytosolic isoforms (creatine kinase brain-type (CKB) and creatine kinase muscle-type (CKM)) and two mitochondrial isoforms (mitochondrial creatine kinase ubiquitous-type (CKMT1) and mitochondrial creatine kinase sarcomeric type (CKMT2)).[3] CKB/CKM and CKMT1/CKMT2 converts cytosolic ATP generated from glycolysis and mitochondria ATP produced by oxidative phosphorylation to PCr for energy storage, respectively, while some cytosolic CK, associated with ATP-consuming processes involving ATPases, ATP-dependent ion channels and transporters, and ATP-requiring metabolic enzymes and protein kinases, regenerates ATP from cytosolic PCr for prompt energy utilization.[4]

Thus the Cr/PCr circuit mediated by CK becomes a fundamental energy regulation system functioning in spatial and temporal energy buffering to maintain cellular ATP concentrations, especially in rapid ATP-consuming tissues, such as the brain, heart, and skeletal muscle. Deficiency of CK in mice causes dampened muscle burst activity, abnormal brain morphology, and severely impaired spatial learning.[5,6] In addition, CK also functions in futile creatine cycling for adipocyte thermogenesis,[7,8] T cell development and activation,[9] and cancer cell proliferation and metastasis.[10–13] Although the underlying molecular mechanism of these CK functions is generally attributed to the metabolic reaction between ATP/ADP and Cr/PCr catalyzed by CK to maintain adequate ATP level for immediate or long-term needs, whether or not related to energetics or energy buffering, the distinct mechanistic details or pathways are still not well illustrated under specific circumstances and require further work for elucidation. Nevertheless, there is another possibility that CK might have other unrevealed enzymatic activities.

Notably, it has been pointed out that the metabolic substrates Cr/PCr might have unconventional roles beyond the CK-PCr circuit in energy metabolism to regulate tumor growth, modulate chromatin remodeling in macrophage polarization, exert membrane protection, and possess a direct antioxidant effect.[3,4,14–20] Thus potential activities and functions of CK or Cr/PCr independently of CK-PCr circuit are drawing great interests.

[1]Interdisciplinary Research Center on Biology and Chemistry, Shanghai Institute of Organic Chemistry, Chinese Academy of Sciences, Shanghai 201210, China

[2]Shanghai Key Laboratory of Regulatory Biology, Institute of Biomedical Sciences, School of Life Sciences, East China Normal University, Shanghai 200241, China

[3]University of Chinese Academy of Sciences, Beijing 100049, China

[4]These authors contributed equally

[5]Lead contact

*Correspondence: hongjiang@sioc.ac.cn

https://doi.org/10.1016/j.isci.2023.106684

Here we demonstrate that CKB might act as a protein kinase to regulate BCAR1 tyrosine phosphorylation using PCr as the phosphate donor by *in vitro*/in-cell phosphorylation assays, quantitative phosphoproteomics, and cellular experiments. Moreover, phosphorylated BCAR1 associates with RBBP4 more favorably to form a complex, which is recruited to the promoter regions of some DNA damage repair genes, such as *RAD51*, to stimulate DNA damage repair. Thus CKB-BCAR1-RBBP4 pathway may play a functional role in DNA damage repair. These findings discover the non-metabolic activities and functions of CK/PCr and the previously unrecognized role of BCAR1 in transcriptional regulation.

RESULTS

Creatine kinase brain-type catalyzes the phosphorylation of BCAR1 at Y327

Because CK catalyzes the transfer of a high-energy phosphate from PCr to ADP generating ATP, we speculate that CK might have some capacity to transfer the high-energy phosphate from PCr to protein tyrosine residues under certain circumstances. To test this hypothesis, we carried out *in vitro* phosphorylation reactions, using recombinant His-CKB purified from *E. coli* as the protein kinase, Mg^{2+} as the catalytic metal ion for CKB, PCr as the phosphate donor, and 293T CKB knockdown (KD) or CKB/CKM double knockdown (DKD) cell lysate (dialyzed to remove endogenous small molecules including ATP) as the source of substrate proteins (Figures S1A and S1B). The reaction mixture was examined by western blot (WB) using the phosphotyrosine (pY) antibody to detect the positive pY signals compared with negative controls in which there was no His-CKB or PCr or Mg^{2+}. The results clearly illustrated that there are significant positive pY signals (>50 kD) with the presence of His-CKB in the reaction comparing with negative controls (Figures 1A, 1B, and S1C), implying that CKB might use PCr to phosphorylate some proteins in cell lysate. It is noticed that pY signals of proteins smaller than 50 kD, originating from endogenous phosphorylated proteins in cell lysates, weren't affected by His-CKB or PCr markedly, although these pY signals were more obvious sometimes. Because there is still some residue of endogenous CKB in 293T CKB KD cell lysate comparing with CKB/CKM DKD cell lysate (Figures S1A and S1B), some extra pY signals (>50 kD) were observed in the sample without recombinant His-CKB (S2) comparing with the sample without PCr (S3) in Figure 1A using 293T CKB KD cell lysate, but not in Figure 1B using CKB/CKM DKD cell lysate, which suggests CKB could positively regulate tyrosine phosphorylation of some proteins.

Most importantly, both CKB inhibitor cyclo-creatine (Cyclo-Cr) and CKB catalytic mutants (R292Q, R292K, or C283S) diminished pY signals (Figures 1B, 1C, S1C, and S1D), further supporting that CKB might act as a protein kinase using PCr as the phosphate donor.

To find out the identities of phosphotyrosine proteins regulated by CKB and PCr, the phosphorylated proteins in the reactions (S1 to S4 in Figure 1A) were enriched by phosphotyrosine antibody for mass spectrometry (MS) identification (Figure 1D) (Data S1). Proteins with enrichment ratios (S1/S2) > 3, (S1/S3) > 10 and (S1/S4) > 10 were considered as positive hits. We obtained total of 10 proteins as positive hits from the phosphoproteomics data (Figure 1E) (Data S1). Among these proteins, BCAR1 (p130Cas), as an adaptor protein mediating multiple signaling pathways to modulate cell motility, cell cycle, cell transformation, and apoptosis,[21–24] was selected for further validation.

As shown in Figure 1F, *in vitro* phosphorylation assay verified that recombinant BCAR1-Flag (purified from 293T CKB/CKM DKD cells) could be tyrosine-phosphorylated by His-CKB WT, but not His-CKB catalytic mutants (R292Q, R292K, or C283S), together with PCr.

BCAR1 has a substrate domain (SD, 115-416aa), which contains 18 Tyr/Y residues (including 15 YxxP repeats) as the potential tyrosine-phosphorylation sites.[21,23,24] Mutation of all 18 Tyr in BCAR1 substrate domain to Phe/F (SD-18F) diminished tyrosine-phosphorylation signal (Figure 1G), implying that the potential phosphorylation site is within these Tyr residues. From screening each single Y to F mutant of BCAR1 substrate domain by *in vitro* phosphorylation assay (Figures 1G and S2A-S2F), Y327F mutant abrogated phosphorylation dramatically and consistently meaning that BCAR1 may be phosphorylated mainly at Y327 by CKB and PCr.

In order to validate BCAR1 Y327 is the phosphorylation site, we generated site-specific BCAR1 pY327 antibody to facilitate the detection (Figures S3A and S3B). As shown in Figure 1H, BCAR1 pY327 signal is enhanced significantly with the presence of CKB and PCr, but not CKB or PCr alone, further supporting that CKB may phosphorylate BCAR1 at Y327 using PCr.

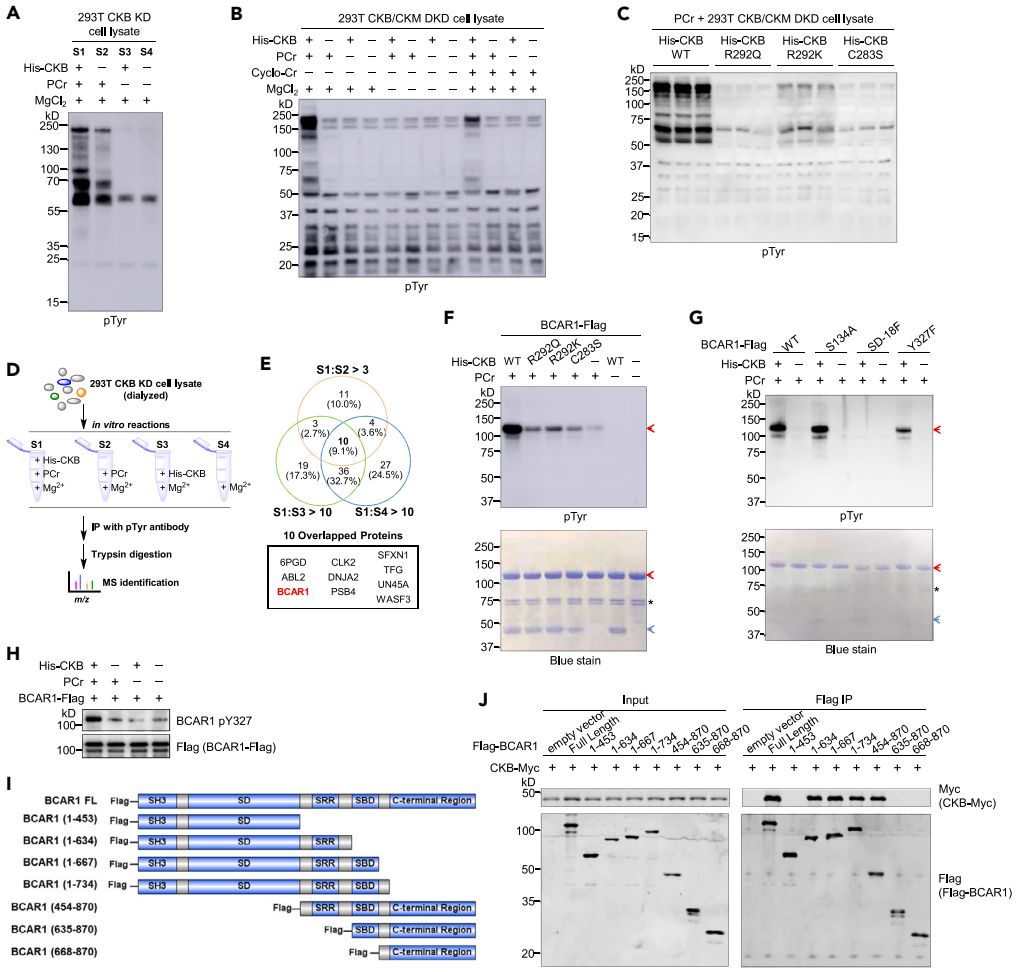

Figure 1. CKB catalyzes the phosphorylation of BCAR1 at Y327

(A and C) *In vitro* phosphorylation assays analyzed by pTyr WB. (A) Dialyzed 293T CKB KD cell lysate was treated with or without His-CKB or PCr in the presence of $MgCl_2$; (B) Dialyzed 293T CKB/CKM DKD cell lysate was treated with or without His-CKB, PCr, $MgCl_2$ or Cyclo-Cr; and (C) Dialyzed 293T CKB/CKM DKD cell lysate was treated with His-CKB WT/R292Q/R292K/C283S, PCr, and $MgCl_2$. Cell lysates (2 μg/μL), PCr (1 mM), $MgCl_2$ (5 mM), Cyclo-Cr (2 mM) and His-CKB WT/mutants (0.4 μg/μL in A and C, 2 μg/μL in (B) were used in the assays as indicated. See also Figures S1C and S1D for Blue stain of samples.

(D) Workflow to enrich and identify phosphortyrosine proteins from *in vitro* phosphorylation assays in (A).

(E) Candidate substrates of CKB and PCr are identified from MS experiments with the cutoff ratios (S1/S2 > 3, S1/S3 > 10, and S1/S4 > 10) (see also Supplemental File Data S1). The overlapped proteins are considered positive targets and listed.

(F-H) *In vitro* phosphorylation assays for purified BCAR1 proteins. (F) Purified BCAR1-Flag was treated with His-CKB WT/R292Q/R292K/C283S, PCr, and $MgCl_2$ before examined by pTyr WB; (G) Purified BCAR1-Flag (WT or mutants) was treated with or without His-CKB in the presence of PCr and $MgCl_2$ before examined by pTyr WB; and (H) Purified BCAR1-Flag was treated with or without His-CKB or PCr in the presence of $MgCl_2$, and then examined by BCAR1 pY327 WB after IP with pTyr antibody. Purified BCAR1-Flag WT/mutants (2 μg/μL), PCr (5 mM in F and G, 1 mM in H), $MgCl_2$ (5 mM), and His-CKB WT/mutants (1 μg/μL) were used in the assays as indicated. See also Figure S2 for more *in vitro* phosphorylation assays.

(I) Diagram of full length (FL) and various truncations of Flag-BCAR1 for co-IP experiments in cells. BCAR1 contains five domains: SH3, SD, SRR, SBD, and C-terminal Region.

(J) Mapping of BCAR1 interacting domain by co-IP of various constructs of Flag-BCAR1 with CKB-Myc in 293T cells. In the WB and protein gels, red arrows and blue arrows point at the positions of BCAR1-Flag and His-CKB, respectively, and asterisk marks the non-specific proteins. See also Figures S1-S3.

Moreover, co-immunoprecipitation (co-IP) experiments were carried out with CKB-Myc and various truncations of Flag-BCAR1 expressed in 293T CKB/CKM DKD cells (Figures 1I and 1J). The results demonstrate that serine-rich region (SRR) of BCAR1 mediates its interaction with CKB.

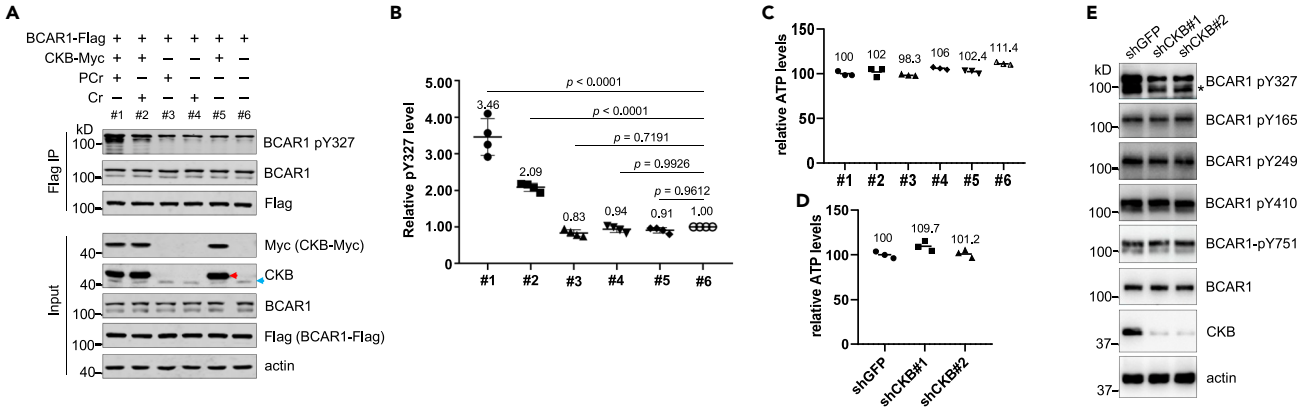

Figure 2. Regulation of BCAR1 Y327 phosphorylation by CKB and PCr in cells and *in vivo*

(A) In-cell phosphorylation assays analyzed by BCAR1 pY327 WB. BCAR1-Flag was immunoprecipitated from 293T CKB/CKM DKD cells overexpressing BCAR1-Flag and CKB-Myc in the absence or presence of 1 mM PCr/Cr. The red arrow and blue arrow point at the positions of CKB-Myc and endogenous CKB, respectively.

(B) Relative pY327 levels in (A). The data are presented as mean ± SD from four independent experiments (n = 4) and analyzed by Student's t tests.

(C and D) Relative ATP levels in: (C) cells from experiments in (A); and (D) MCF-7 shGFP/shCKB#1/shCKB#2 cells. The data are presented as mean ± SD from three independent experiments (n = 3).

(E) Detection of endogenous BCAR1 pY327 in MCF-7 shGFP/shCKB#1/shCKB#2 cells. Asterisk marks the position of truncated BCAR1.

BCAR1 pY327 level is modulated by creatine kinase brain-type and phosphocreatine in cells and *in vivo*

To investigate whether BCAR1 pY327 in cells is regulated by CKB and PCr, in-cell phosphorylation assay was executed. 293T CKB/CKM DKD cells, which had been cultured with dialyzed FBS to remove endogenous Cr and PCr, were used in the assay. BCAR1-Flag, with or without CKB-Myc, was overexpressed in the cells in the presence or absence of exogenous Cr or PCr, and then isolated by Flag IP for BCAR1 pY327 WB. In accordance with *in vitro* phosphorylation (Figure 1H), BCAR1 pY327 is notably upregulated when both CKB-Myc and exogenous PCr are present (Figures 2A and 2B), while cellular ATP doesn't increase actually (Figure 2C), indicating that CKB and PCr may directly regulate BCAR1 pY327 in cells.

In addition, deficiency of CKB in MCF-7 cells, which doesn't decrease cellular ATP (Figure 2D), evidently reduced BCAR1 pY327 level but not other known pY residues (Figure 2E), meaning endogenous CKB specifically regulates endogenous BCAR1 pY327 in cells.

BCAR1 Y327 phosphorylation augments its association with RBBP4

To figure out the functional role of BCAR1 pY327, IP-MS of BCAR1-Flag WT and Y327F (phosphordeficient mutant) from 293T cells was carried out to identify the interacting proteins specific for BCAR1 pY327 (Figures 3A and S3C) (Data S2). From the analysis (Figure 3B), proteins with ratio BCAR1 WT/Y327F > 5 and p value <0.01 (categorized in the "UP" group) were considered as the potential interactors specific for BCAR1 pY327, in which RBBP4 (retinoblastoma binding proteins 4, also known as RbAp48), a histone-binding protein involved in chromatin remodeling and histone modifications,[25–28] is identified.

To validate the interaction between BCAR1 and RBBP4, co-IP experiments of RBBP4-Myc with BCAR1-Flag WT, Y327F, or Y327E (phosphomimetic mutant) in 293T cells were performed. As shown in Figure 3C, BCAR1-Flag WT indeed pulled down more RBBP4-Myc than BCAR1-Flag Y327F, in line with the IP-MS result (Figure 3B), and further BCAR1-Flag Y327E, which mimics Y327 phosphorylation, captured the most amount of RBBP4. These results clearly demonstrated that BCAR1 interacts with RBBP4 in cells and, most importantly, Y327 phosphorylation improves their association markedly.

Correspondingly, co-IP experiments of RBBP4-Myc with various truncations of Flag-BCAR1 in 293T cells indicate that RBBP4 interacts with the SH3-SD domain of BCAR1 which contains Y327 residue (Figures 1I and 3D), supporting the regulatory role of Y327 phosphorylation in the association between BCAR1 and RBBP4.

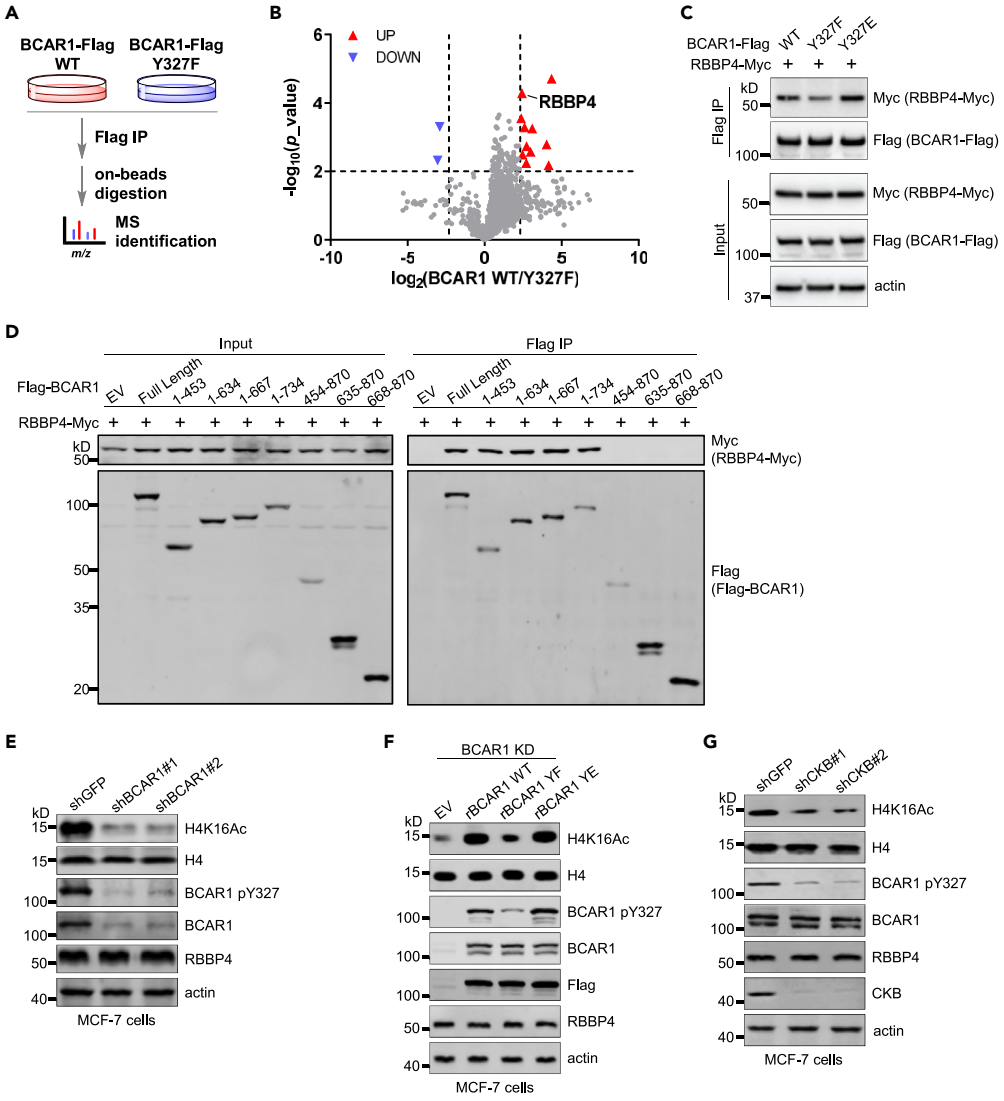

Figure 3. BCAR1 associates with RBBP4 to modulate H4K16Ac level

(A) Workflow to carry out IP-MS of BCAR1-Flag WT and Y327F from 293T cells.

(B) Statistical analysis of IP-MS results from (A) (see also Data S2). Proteins with "ratio BCAR1 WT/Y327F > 5, p value <0.01" or "ratio BCAR1 WT/Y327F < 0.20, p value <0.01" are categorized in "UP" or "Down" group, respectively.

(C) Co-IP experiments of RBBP4-Myc with BCAR1-Flag WT, Y327F, or Y327E in 293T cells.

(D) Mapping of BCAR1 interacting domain by co-IP of various constructs of Flag-BCAR1 with RBBP4-Myc in 293T cells.

(E-G) Examination of H4K16Ac levels in: (E) MCF-7 shGFP, shBCAR1#1 or shBCAR1#2 cells; (F) MCF-7 BCAR1 KD cells rescued with rBCAR1-Flag WT/Y327F/Y327E or empty vector (EV); and (G) MCF-7 shGFP, shCKB#1, or shCKB#2 cells. See also Figure S3.

BCAR1 binds to the RAD51 promoter to regulate its transcription together with RBBP4

RBBP4, as a key component in various complexes, has a pivotal role in transcription regulation by modulating histone acetylation.[27,29–32] Since BCAR1 interacts with RBBP4 and BCAR1 Y327 phosphorylation enhances its association with RBBP4, it is conceivable that BCAR1 and its Y327 phosphorylation might affect histone acetylation via RBBP4.

Indeed, the H4K16Ac level is dramatically reduced in BCAR1 KD cells (Figure 3E). And rescue with shRNA-resistant BCAR1-Flag WT (rBCAR1 WT) or Y327E (rBCAR1 YE), which bears higher level of Y327 phosphorylation comparing with shRNA-resistant BCAR1-Flag Y327F (rBCAR1 YF), effectively stimulated H4K16Ac level (Figure 3F).

Furthermore, the H4K16Ac level decreased evidently with CKB knockdown in MCF-7 cells coinciding with lower level of endogenous BCAR1 pY327 (Figure 3G). These results suggest that BCAR1 Y327 phosphorylation may upregulate the H4K16Ac level by association with more RBBP4.

It is reported that RBBP4 interacts with CBP/p300 to facilitate histone lysine acetylation and activate the transcription of *MGMT* and *RAD51*, two key DNA repair genes, by binding to their promoters.[30] Thus we hypothesize that BCAR1 may participate in RBBP4-CBP/p300 complex and be recruited to *MGMT* and *RAD51* promoters.

To testify this hypothesis, sequential chromatin immunoprecipitation (ChIP re-ChIP) was carried out in 293T cells with co-expression of RBBP4-Myc and BCAR1-Flag WT or Y327F. After an initial Flag ChIP to capture BCAR1-Flag WT or Y327F bound chromatin, RBBP4-Myc bound chromatin was re-ChIPed from the original Flag ChIP using Myc antibody. Then isolated DNA fragments in the promoter regions of *RAD51* and *MGMT* were quantified by qPCR. As shown in Figure 4A, there are higher levels of promoter DNA fragments of both *RAD51* and *MGMT* in BCAR1 WT samples than in BCAR1 Y327F samples, implying that BCAR1 Y327 phosphorylation promotes BCAR1 bound to RAD51 and MGMT promoters in complex with RBBP4.

To further examine the levels of H4K16Ac and BCAR1-RBBP4 complex in the RAD51 promoter region, ChIP-qPCR was performed in MCF-7 BCAR1 KD cells rescued with shRNA-resistant BCAR1-Flag WT (rBCAR1 WT), Y327F (rBCAR1 YF) or GFP-Flag, using RBBP4, H4K16Ac or Flag antibody, respectively. Intriguingly, levels of BCAR1, RBBP4, and H4K16Ac in the RAD51 promoter region are significantly higher in rBCAR1 WT cells than in rBCAR1 YF cells (Figure 4B). Furthermore, deprivation of CKB in MCF-7 cells greatly reduced the levels of RBBP4 and H4K16Ac in the RAD51 promoter region (Figure 4C). These findings confirm that BCAR1 Y327 phosphorylation, regulated by CKB, facilitates BCAR1-RBBP4 complex formation and its recruitment to the *RAD51* promoter to elevate the H4K16Ac level.

Consequently, under the same circumstance, mRNA level of RAD51 increased in rBCAR1 WT cells or declined in CKB KD cells (Figures 4D and 4E).

We carried out additional ChIP assays in RBBP4 KD cells overexpressing BCAR1-Flag WT/Y327F(YF) or GFP-Flag comparing with controls (Figure 4F). In Flag ChIP results, comparing with GFP-Flag, BCAR1-Flag WT, and YF still associate with RAD51 promoter in RBBP4 KD cells, indicating that BCAR1 could bind to RAD51 promoter independently of RBBP4. And there is no difference between BCAR1 WT and YF in RBBP4 KD cells meaning that Y327 phosphorylation doesn't affect this RBBP4-independent binding of BCAR1 to RAD51 promoter.

Furthermore, BCAR1 WT has significantly higher binding to RAD51 promoter in shGFP cells than BCAR1 YF in shGFP cells and BCAR1 WT in RBBP4 KD cells, while only slightly more BCAR1 YF associates at RAD51 promoter in shGFP cells than in RBBP4 KD cells. These data reveal that the presence of RBBP4 could elevate the binding of BCAR1 to RAD51 promoter and BCAR1 Y327 phosphorylation, which enhances the association between BCAR1 and RBBP4, could further promote more BCAR1 binding to RAD51 promoter markedly.

In H4K16Ac ChIP results, there is no difference in RBBP4 KD cells overexpressing BCAR1-Flag WT/YF or GFP-Flag. This indicates that BCAR1 alone couldn't affect the H4K16Ac level at the RAD51 promoter when RBBP4 is absent, despite BCAR1 association at the RAD51 promoter. And in shGFP cells, BCAR1 WT, but not YF, could upregulate the H4K16Ac level comparing with GFP, which validates that only BCAR1 Y327 phosphorylation, not BCAR1 without pY327, promotes the H4K16Ac level. In other words, no BCAR1 Y327 phosphorylation and no elevation of the H4K16Ac level.

Collectively, the above ChIP assays demonstrate that BCAR1 could bind to RAD51 promoter independently of RBBP4, and Y327 phosphorylation increases BCAR1 association with RAD51 promoter in the presence of RBBP4, while RBBP4 binding to RAD51 promoter depends on BCAR1 Y327 phosphorylation. And further H4K16Ac level is promoted by BCAR1 Y327 phosphorylation via RBBP4.

Moreover, at the protein level, RAD51 has a lower expression with BCAR1 deficiency (Figure 5A), and could be elevated remarkably with rBCAR1 WT/YE complementation (Figure 5B), consistent with H4K16Ac and

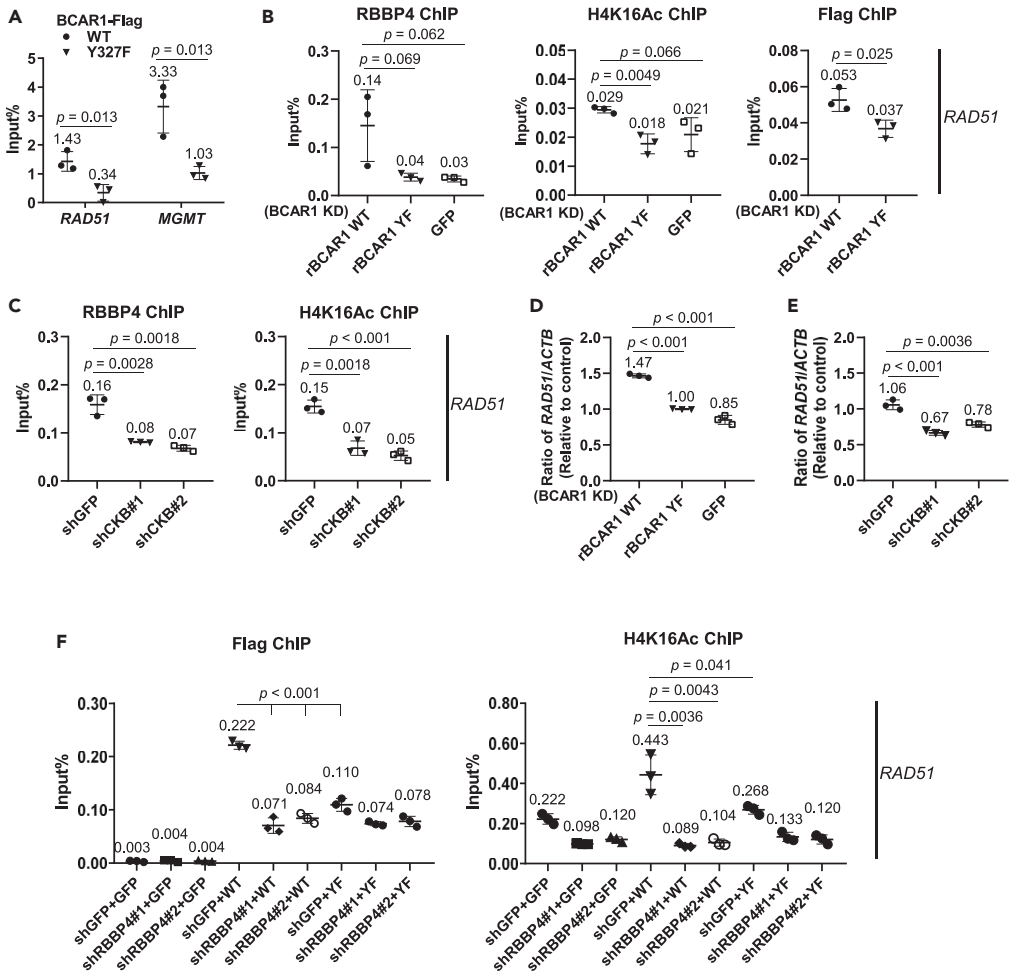

Figure 4. BCAR1 binds to the promoter region of *RAD51* to regulate its transcription together with RBBP4

(A) ChIP re-ChIP assay. The assay was carried out to evaluate the coexistence of BCAR1 and RBBP4 in the promoter regions of *RAD51* and *MGMT* in 293T cells co-transfected with RBBP4-Myc and BCAR1-Flag WT/Y327F.

(B and C) ChIP assays were performed: (B) to examine H4K16Ac modification and the existence of BCAR1 or RBBP4 in the promoter region of *RAD51* in MCF-7 BCAR1 KD cells rescued with rBCAR1-Flag WT/Y327F or GFP-Flag; and (C) to examine H4K16Ac modification and the existence of RBBP4 in the promoter region of *RAD51* in MCF-7 shGFP, shCKB#1 or shCKB#2 cells.

(D and E) mRNA levels of *RAD51* in: (D) MCF-7 BCAR1 KD cells rescued with rBCAR1-Flag WT/Y327F or GFP-Flag; and (E) MCF-7 shGFP, shCKB#1 or shCKB#2 cells.

(F) ChIP assays were performed to examine H4K16Ac modification and the existence of BCAR1-Flag WT/Y327F(YF) in the promoter region of *RAD51* in MCF-7 shGFP, shRBBP4#1 or shRBBP4#2 cells overexpressing BCAR1-Flag WT/Y327F(YF) or GFP-Flag Cells were cultured with 5 ng/mL TGF-β for 24 h before examination. The data in all figures are presented as mean ± SD from three independent experiments (n = 3) and analyzed by Student's t tests.

BCAR1 pY327 levels. Lack of CKB also reduced RAD51 expression (Figure 5C), presumably due to down-regulated BCAR1 pY327. Thus rescue with BCAR1 Y327E, but not BCAR1 WT or Y327F, in MCF-7 CKB KD cells increased expressions of RAD51 and H4K16Ac (Figure 5D), since BCAR1 Y327E mimics Y327 phosphorylation and BCAR1 WT has low pY327 level, same as Y327F, without CKB. These data clarify that BCAR1 Y327 phosphorylation upregulates RAD51 transcription and protein expression.

Notably, when RBBP4 is absent, both H4K16Ac and RAD51 are dampened, which are not affected by BCAR1 Y327 phosphorylation even with overexpression of BCAR1 WT/Y327E (Figures 5E and 5F). This verifies that the regulation of RAD51 and H4K16Ac by BCAR1 Y327 phosphorylation is mediated by RBBP4.

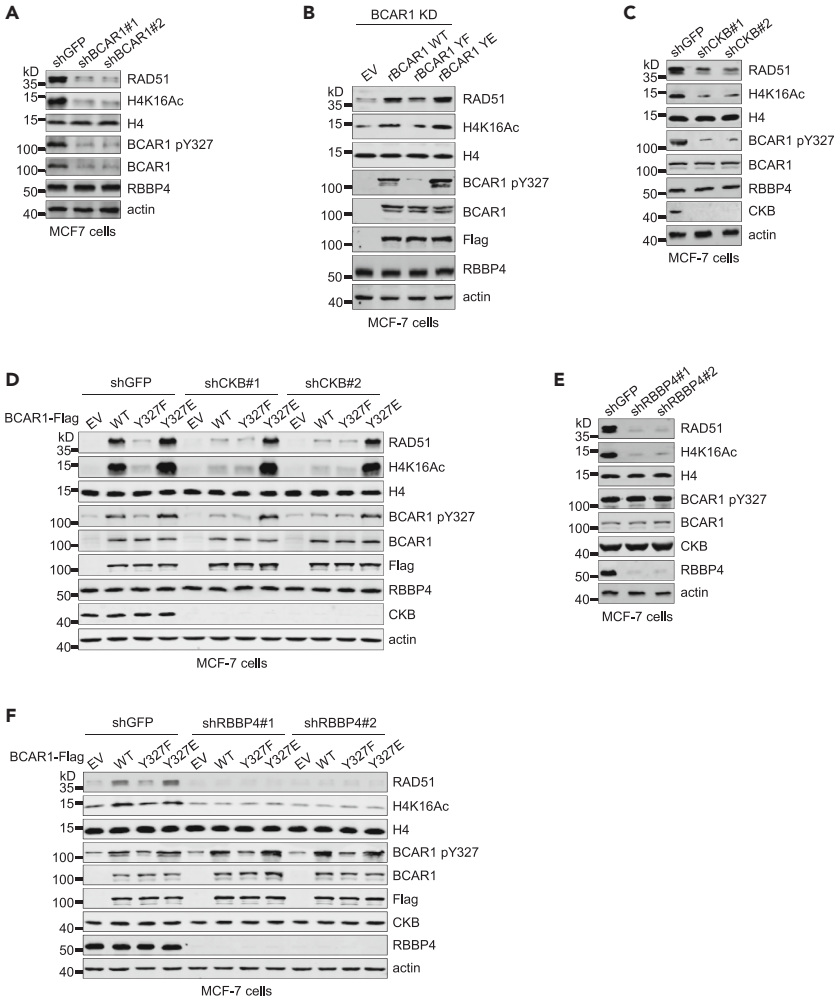

Figure 5. BCAR1 Y327 phosphorylation elevates RAD51 expression and H4K16Ac level mediated by RBBP4

(A-F).WB analysis of RAD51 and H4K16Ac levels in: (A) MCF-7 shGFP, shBCAR1#1 or shBCAR1#2 cells; (B) MCF-7 BCAR1 KD cells rescued with rBCAR1-Flag WT/Y327F/Y327E or empty vector (EV); (C) MCF-7 shGFP, shCKB#1 or shCKB#2 cells; (D) MCF-7 shGFP, shCKB#1 or shCKB#2 cells overexpressing BCAR1-Flag WT/Y327F/Y327E or empty vector (EV); (E) MCF-7 shGFP, shRBBP4#1 or shRBBP4#2 cells; and (F) MCF-7 shGFP, shRBBP4#1 or shRBBP4#2 cells overexpressing BCAR1-Flag WT/Y327F/Y327E or empty vector (EV).

BCAR1 Y327 phosphorylation promotes DNA damage repair

Because RAD51 is essential in the homologous recombination (HR) pathway during DNA double-strand break (DSB) repair,[33,34] it is reasonable to speculate that BCAR1 Y327 phosphorylation is also involved in DNA damage repair. To investigate the effects on DNA damage repair by BCAR1 Y327 phosphorylation, comet assay, or single cell gel electrophoresis, is applied to evaluate DNA fragmentation.

As illustrated in Figures 6A and S4A, tail moment, as the indicator of DNA damage, is shorter in MCF-7 cells stably expressing BCAR1 WT/Y327E than in MCF-7 cells stably expressing BCAR1 Y327F under etoposide treatment, coinciding with more RAD51 and less γH2AX (a biomarker of DNA damage) in these cells (Figure 6B), implying that BCAR1 Y327 phosphorylation enhances DNA damage repair.

Similarly, rescue by rBCAR1 WT/Y327E in MCF-7 BCAR1 KD cells boosted RAD51 expression and improved DNA damage repair resulting in shorter tail moments and lower γH2AX level, in comparison with rescue by rBCAR1 Y327F (Figures 6C, 6D and S4B). Furthermore, longer tail moments and higher γH2AX levels, together with reduced RAD51, were observed in MCF-7 CKB KD cells (shCKB#1 and shCKB#2) demonstrating that CKB deficiency in MCF-7 cells impaired DNA damage repair (Figures 6E, 6F, and S4C). And complementation of

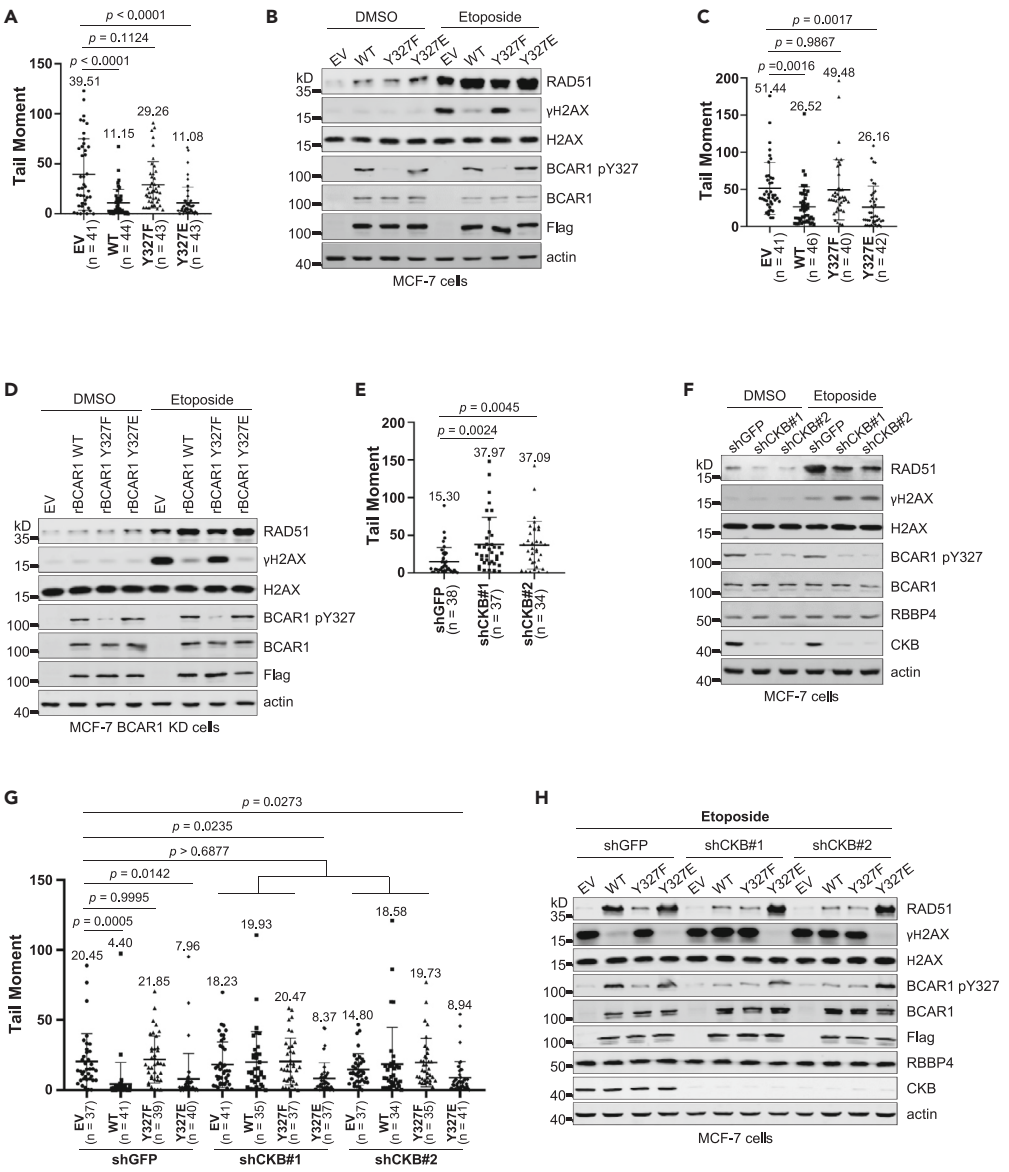

Figure 6. BCAR1 Y327 phosphorylation promotes DNA damage repair

(A, C, E and G) Comparison of tail moments in comet assays for: (A) MCF-7 cells stably overexpressing BCAR1-Flag WT/Y327F/Y327E or empty vector (EV) (n = 41, 44, 43 and 43 for EV, BCAR1 WT, Y327F, and Y327E, respectively); (C) MCF-7 BCAR1 KD cells rescued with rBCAR1-Flag WT/Y327F/Y327E or empty vector (EV) (n = 41, 46, 40 and 42 for EV, BCAR1 WT, Y327F, and Y327E, respectively); (E) MCF-7 shGFP, shCKB#1 or shCKB#2 cells (n = 38, 37 and 34 for shGFP, shCKB#1 and shCKB#2, respectively); (G) MCF-7 shGFP, shCKB#1 or shCKB#2 cells overexpressing BCAR1-Flag WT/Y327F/Y327E or empty vector (EV) (n = 37, 41, 39 and 40 for EV, BCAR1 WT, Y327F, and Y327E in shGFP cells, respectively; n = 41, 35, 37 and 37 for EV, BCAR1 WT, Y327F, and Y327E in shCKB#1 cells, respectively; n = 37, 34, 35 and 41 for EV, BCAR1 WT, Y327F, and Y327E in shCKB#2 cells, respectively). The data are presented as mean ± SD and analyzed by Student's t tests. (B, D, F, and H) WB analysis of RAD51 and γH2AX in: (B) MCF-7 cells stably overexpressing BCAR1-Flag WT/Y327F/Y327E or empty vector (EV); (D) MCF-7 BCAR1 KD cells rescued with rBCAR1-Flag WT/Y327F/Y327E or empty vector (EV); (F) MCF-7 shGFP, shCKB#1 or shCKB#2 cells; (H) MCF-7 shGFP, shCKB#1 or shCKB#2 cells overexpressing BCAR1-Flag WT/Y327F/Y327E or empty vector (EV) Cells in (A-H) were treated with 20 μM etoposide or DMSO for 4 h before examination. See also Figure S4.

MCF-7 CKB KD cells with BCAR1 Y327E, but not BCAR1 WT or Y327F, improved RAD51 expression and DNA damage repair significantly with diminished γH2AX (Figures 6G, 6H and S4D), illustrating the essential role of Y327 phosphorylation in the regulation of RAD51-mediated DNA damage repair.

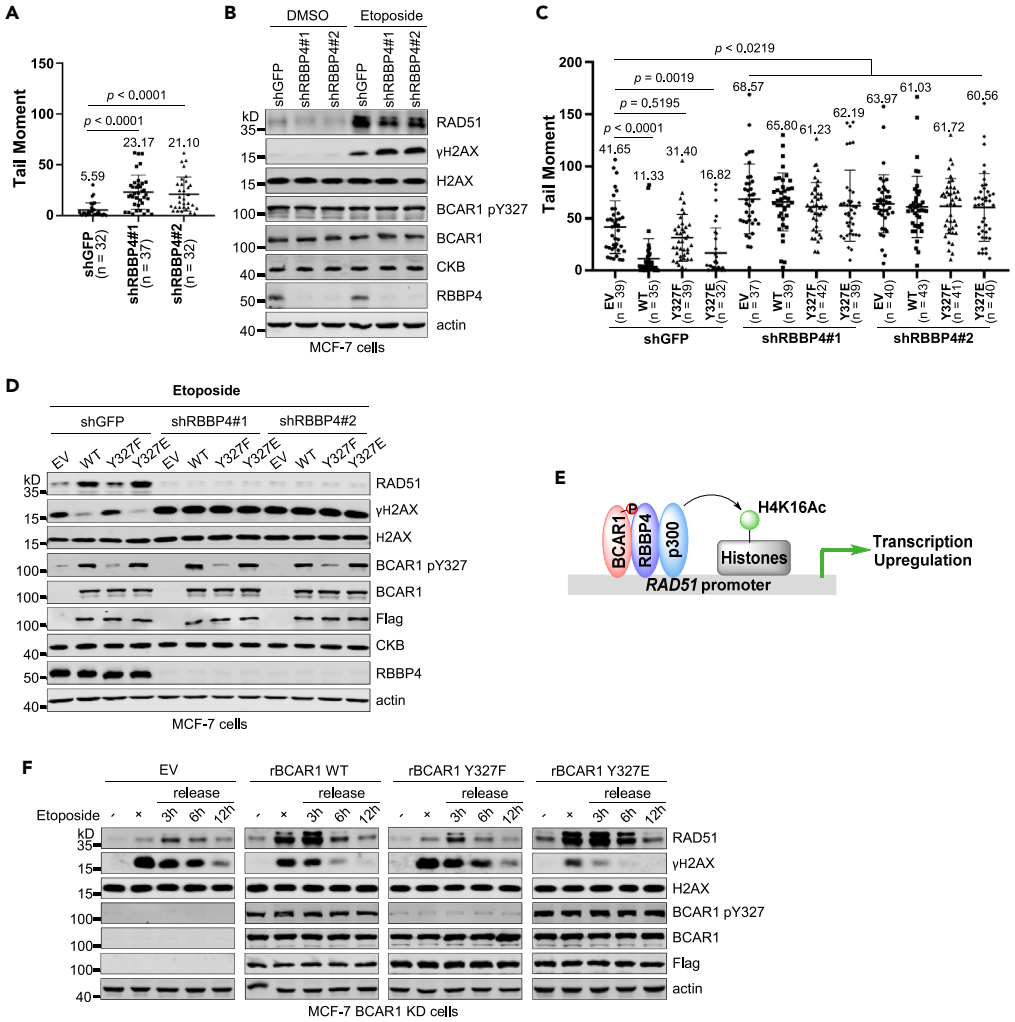

Figure 7. RBBP4 mediates the promotion of DNA damage repair by BCAR1 Y327 phosphorylation

(A and C) Comparison of tail moments in comet assays for: (A) MCF-7 shGFP, shRBBP4#1 or shRBBP4#2 cells (n = 32, 37 and 32 for shGFP, shRBBP4#1 and shRBBP4#2, respectively); and (C) MCF-7 shGFP, shRBBP4#1 or shRBBP4#2 cells overexpressing BCAR1-Flag WT/Y327F/Y327E or empty vector (EV) (n = 39, 35, 39 and 32 for EV, BCAR1 WT, Y327F, and Y327E in shGFP cells, respectively; n = 37, 39, 42 and 39 for EV, BCAR1 WT, Y327F, and Y327E in shRBBP4#1 cells, respectively; n = 40, 43, 41 and 40 for EV, BCAR1 WT, Y327F, and Y327E in shRBBP4#2 cells, respectively). The data are presented as mean ± SD and analyzed by Student's t tests.

(B and D) WB analysis of RAD51 and γH2AX in: (B) MCF-7 shGFP, shRBBP4#1 or shRBBP4#2 cells; and (D) MCF-7 shGFP, shRBBP4#1 or shRBBP4#2 cells overexpressing BCAR1-Flag WT/Y327F/Y327E or empty vector (EV).

(E) A proposed model that BCAR1 Y327 phosphorylation facilitates the association with RBBP4 and its recruitment to *RAD51* promoter to enhance H4K16 acetylation leading to transcriptional upregulation.

(F) WB analysis of RAD51 and γH2AX in MCF-7 BCAR1 KD cells rescued with rBCAR1-Flag WT/Y327F/Y327E or empty vector (EV) Cells in (A-D) were treated with 20 μM etoposide or DMSO for 4 h before examination. Cells in (F) were treated with 20 μM etoposide for 4 h and then released into the fresh medium without etoposide for indicated times. See also Figure S4.

Importantly, depletion of RBBP4 diminished RAD51 protein level and impaired DNA damage repair as shown by longer tail moments and higher γH2AX levels (Figures 7A, 7B, and S4E). In addition, the absence of RBBP4 abolished the benefits of BCAR1 WT/Y327E overexpression for DNA damage repair in MCF-7 cells, because there were significantly higher expression of RAD51, resulting in shorter tail moments and lower γH2AX level, with overexpression of BCAR1 WT/Y327E than BCAR1 Y327F in GFP KD cells (shGFP) but not in RBBP4 KD cells (shRBBP4#1 and shRBBP4#2) (Figure 7C, 7D, and S4F). These results corroborate that BCAR1 Y327 phosphorylation promotes DNA damage repair which is mediated by RBBP4 (Figure 7E).

To investigate the influence of BCAR1 Y327 phosphorylation on DNA repair kinetics, MCF-7 BCAR1 KD cells rescuing with rBCAR1 WT/Y327F/Y327E were treated with etoposide and then released into fresh medium without etoposide for indicated times. As shown in Figure 7F, RAD51 was elevated more dramatically and maintained at higher protein level for longer time with rBCAR1 WT/Y327E complementation, comparing with rBCAR1 Y327F complementation or empty vector (EV) control, while γH2AX appeared less and diminished more quickly at the same time, further emphasizing the beneficial role of BCAR1 Y327 phosphorylation in DNA damage repair.

DISCUSSION

As a key regulator in energy metabolism, CK has been considered essential to maintain energy homeostasis for normal functions of organs. Higher expression of CK in cancer cells also emphasizes the importance of its metabolic activity in energetics for cancer cell survival, proliferation, and metastasis. Thus the non-metabolic activity of CK seems to be masked. Considering that PCr, the metabolic substrate of CK, has one high-energy phosphate group for transfer to ADP and the cellular concentration of PCr could reach to 20-30 mM,[4,35–37] there may be a possibility that CK could transfer the high-energy phosphate group to the protein residues under certain circumstances.

Similar to some metabolic enzymes, including pyruvate kinase M2 (PKM2),[38,39] phosphoglycerate kinase 1 (PGK1),[40] fructokinase A (ketohexokinase A, KHK-A),[41] phosphoenolpyruvate carboxykinase 1 (PCK1)[42] and choline kinase α2 (CHKα2),[43] which could behave as protein kinases to modify proteins, CKB was shown to phosphorylate BCAR1 using PCr as the phosphate donor in this study. Our data provide evidence that CKB has non-metabolic activity and PCr could participate in protein phosphorylation that is independent on CK/PCr circuit, and also implies that other isoforms of CK might have protein kinase activity as well.

Tyrosine phosphorylation of BCAR1 SD domain (containing 15 repeats of YxxP motif) is mainly catalyzed by Src family kinases and crucial for its functions.[21,23,24] Among these YxxP repeats, phosphorylation of Y165, Y249, and Y410 are mostly referred to as the marker of BCAR1 tyrosine phosphorylation catalyzed by Src. However, the phosphorylation of Y327 hasn't been paid attention to and its specific function was not known until demonstrated to enhance the association of BCAR1 with RBBP4 for the chromatin recruitment in this study. We validated the BCAR1 pY327 level in cells could be regulated by CKB and PCr, consistent with *in vitro* phosphorylation catalyzed by CKB and PCr, without perturbing phosphorylation level of other tyrosine residues in the SD domain, which indicates that pY327 mediated by CKB and PCr is a unique event distinct from phosphorylation executed by Src family kinases.

Although BCAR1 mainly localizes in cytoplasm, it has been demonstrated that BCAR1 can shuttle between cytoplasm and nucleus.[44–46] Nuclear BCAR1 could interact with CBP/p300 to suppress RelA acetylation and then inhibit NF-κB activity,[46] or bind to TP53 mutant to promote cancer cell invasion.[45] Our results verified that BCAR1 and RBBP4 could form a complex to be recruited to the chromatin and co-occupy the promoter regions of some DNA repair genes (Figure 5O), revealing another previously unrecognized function of nuclear BCAR1 in transcriptional regulation and DNA damage repair.

Cancer cells have multiple mechanisms of chemotherapy and radiotherapy resistances, including enhancing DNA damage repair, such as homologous recombination (HR).[47,48] RAD51, as an essential component in the HR pathway, is expressed at high levels in many cancer cells and plays a critical role in cancer progress, metastasis, and chemo-/radioresistance, leading to the poor treatment outcome.[49–51] Thus the downregulation of RAD51 is considered as a promising therapeutic strategy to treat resistant tumors. As we discover that the CKB-BCAR1-RBBP4 pathway could upregulate transcriptional and protein levels of RAD51 and promote DNA damage repair, future comprehensive studies, to investigate the treatment methods either inhibiting BCAR1 phosphorylation mediated by CKB or blocking the association of BCAR1 with RBBP4, may provide potential and valuable adjuvant therapeutic strategies for resistant tumors.

Limitations of the study

Considering *in vitro* phosphorylation assays that we performed in this study, it would be better to reconstitute the reactions using recombinant BCAR1 purified from prokaryotic cells instead of from mammalian cells, to eliminate the effects caused by potential contaminants in the samples originating from mammalian cells. However, we didn't get soluble BCAR1 protein overexpressed from *E. coli* probably due to incorrect protein folding and protein instability. Although we couldn't exclude the possibility that some

contaminants in the purified BCAR1-Flag proteins from 293T CKB/CKM DKD cells might interfere with the *in vitro* results, in-cell phosphorylation assay and cellular experiments undoubtedly demonstrates that BCAR1 pY327 is regulated by CKB.

To verify the effect of BCAR1 pY327 on DNA damage repair, we applied rescue experiments (overexpression of BCAR1 WT/mutants in BCAR1 KD cells lines), which may bring the potential concern about the physiological relevance using overexpression system since the recombinant protein level is obviously higher than the endogenous protein level. It would be more helpful and worthy to carry out knock-in experiment to express the endogenous level of BCAR1 mutants in cells using CRISPR-Cas9 technologies for further investigation and validation.

In addition, it would be more critical to carry out the assays from the cellular level to animal level such as using WT mice and CKB knockout mice to characterize the CKB-BCAR1-RBBP4 pathway in DNA damage repair.

STAR★METHODS

Detailed methods are provided in the online version of this paper and include the following:

- KEY RESOURCES TABLE
- RESOURCE AVAILABILITY
  - Lead contact
  - Materials availability
  - Data and code availability
- EXPERIMENTAL MODEL AND SUBJECT DETAILS
  - Cell lines
- METHOD DETAILS
  - Plasmid construction
  - Dialyzed cell lysates for *in vitro* phosphorylation assay
  - Protein purification of N-His-CKB WT, R292Q, R292K and C283S
  - Protein purification of BCAR1-Flag WT and mutants
  - *In vitro* phosphorylation assay
  - Generation and validation of BCAR1 pY327 antibody
  - Western blotting
  - Co-immunoprecipitation and immunoprecipitation
  - Enrichment of phosphotyrosine proteins for phosphoproteomics
  - IP-MS of BCAR1-Flag WT and Y327F from 293T cells
  - On-beads digestion
  - LC-MS/MS analysis
  - MS data analysis
  - RNA Preparation and RT-PCR
  - ChIP-qPCR assay and ChIP Re-ChIP assay
  - Neutral comet assay
- QUANTIFICATION AND STATISTICAL ANALYSIS

SUPPLEMENTAL INFORMATION

Supplemental information can be found online at https://doi.org/10.1016/j.isci.2023.106684.

ACKNOWLEDGMENTS

We thank Junying Yuan for pLKO.1 vector, pLKO.1-shGFP plasmid and HEK 293T cells; Junhao Hu for psPAX2 and pMD2.G plasmids; and Jidong Zhu for MCF-7 cells. This work was supported by grants from the National Natural Science Foundation of China (No. 21778063 and No. 91753114) to H.J., (No. 32071245) to Y.Z., the Natural Science Foundation of Shanghai (No. 20ZR1474400) to Y.Z., and the Shanghai Municipal Science and Technology Major Project (Grant No. 2019SHZDZX02) to H.J. and Y.Z.

AUTHOR CONTRIBUTIONS

H.J., W.Z., and B.Y. conceived and designed the experiments. H.J. supervised the studies. W.Z. and B.Y. performed the majority of experiments. W.Z., B.Y., B.L., and C.Y. carried out biochemical and cellular

experiments. L.S. and Y.Z. executed protein MS experiments. All the authors analyzed data. H.J. wrote the manuscript with the help from W.Z. and B.Y.

DECLARATION OF INTERESTS

The authors declare no competing interests.

INCLUSION AND DIVERSITY

We support inclusive, diverse, and equitable conduct of research.

Received: February 28, 2023
Revised: March 7, 2023
Accepted: April 13, 2023
Published: April 19, 2023

REFERENCES

1. Wallimann, T., Wyss, M., Brdiczka, D., Nicolay, K., and Eppenberger, H.M. (1992). Intracellular compartmentation, structure and function of creatine kinase isoenzymes in tissues with high and fluctuating energy demands: the 'phosphocreatine circuit' for cellular energy homeostasis. Biochem. J. *281*, 21–40. https://doi.org/10.1042/bj2810021.

2. Wyss, M., and Kaddurah-Daouk, R. (2000). Creatine and creatinine metabolism. Physiol. Rev. *80*, 1107–1213. https://doi.org/10.1152/physrev.2000.80.3.1107.

3. Kazak, L., and Cohen, P. (2020). Creatine metabolism: energy homeostasis, immunity and cancer biology. Nat. Rev. Endocrinol. *16*, 421–436. https://doi.org/10.1038/s41574-020-0365-5.

4. Wallimann, T., Tokarska-Schlattner, M., and Schlattner, U. (2011). The creatine kinase system and pleiotropic effects of creatine. Amino Acids *40*, 1271–1296. https://doi.org/10.1007/s00726-011-0877-3.

5. van Deursen, J., Heerschap, A., Oerlemans, F., Ruitenbeek, W., Jap, P., ter Laak, H., and Wieringa, B. (1993). Skeletal muscles of mice deficient in muscle creatine kinase lack burst activity. Cell *74*, 621–631. https://doi.org/10.1016/0092-8674(93)90510-w.

6. Streijger, F., Oerlemans, F., Ellenbroek, B.A., Jost, C.R., Wieringa, B., and Van der Zee, C.E. (2005). Structural and behavioural consequences of double deficiency for creatine kinases BCK and UbCKmit. Behav. Brain Res. *157*, 219–234. https://doi.org/10.1016/j.bbr.2004.07.002.

7. Streijger, F., Pluk, H., Oerlemans, F., Beckers, G., Bianco, A.C., Ribeiro, M.O., Wieringa, B., and Van der Zee, C.E. (2009). Mice lacking brain-type creatine kinase activity show defective thermoregulation. Physiol. Behav. *97*, 76–86. https://doi.org/10.1016/j.physbeh.2009.02.003.

8. Rahbani, J.F., Roesler, A., Hussain, M.F., Samborska, B., Dykstra, C.B., Tsai, L., Jedrychowski, M.P., Vergnes, L., Reue, K., Spiegelman, B.M., and Kazak, L. (2021). Creatine kinase B controls futile creatine cycling in thermogenic fat. Nature *590*, 480–485. https://doi.org/10.1038/s41586-021-03221-y.

9. Zhang, Y., Li, H., Wang, X., Gao, X., and Liu, X. (2009). Regulation of T cell development and activation by creatine kinase B. PLoS One *4*, e5000. https://doi.org/10.1371/journal.pone.0005000.

10. Fenouille, N., Bassil, C.F., Ben-Sahra, I., Benajiba, L., Alexe, G., Ramos, A., Pikman, Y., Conway, A.S., Burgess, M.R., Li, Q., et al. (2017). The creatine kinase pathway is a metabolic vulnerability in EVI1-positive acute myeloid leukemia. Nat. Med. *23*, 301–313. https://doi.org/10.1038/nm.4283.

11. Kurmi, K., Hitosugi, S., Yu, J., Boakye-Agyeman, F., Wiese, E.K., Larson, T.R., Dai, Q., Machida, Y.J., Lou, Z., Wang, L., et al. (2018). Tyrosine phosphorylation of mitochondrial creatine kinase 1 enhances a druggable tumor energy shuttle pathway. Cell Metabol. *28*, 833–847.e8. https://doi.org/10.1016/j.cmet.2018.08.008.

12. Loo, J.M., Scherl, A., Nguyen, A., Man, F.Y., Weinberg, E., Zeng, Z., Saltz, L., Paty, P.B., and Tavazoie, S.F. (2015). Extracellular metabolic energetics can promote cancer progression. Cell *160*, 393–406. https://doi.org/10.1016/j.cell.2014.12.018.

13. Papalazarou, V., Zhang, T., Paul, N.R., Juin, A., Cantini, M., Maddocks, O.D.K., Salmeron-Sanchez, M., and Machesky, L.M. (2020). The creatine-phosphagen system is mechanoresponsive in pancreatic adenocarcinoma and fuels invasion and metastasis. Nat. Metab. *2*, 62–80. https://doi.org/10.1038/s42255-019-0159-z.

14. Ji, L., Zhao, X., Zhang, B., Kang, L., Song, W., Zhao, B., Xie, W., Chen, L., and Hu, X. (2019). Slc6a8-Mediated creatine uptake and accumulation reprogram macrophage polarization via regulating cytokine responses. Immunity *51*, 272–284.e7. https://doi.org/10.1016/j.immuni.2019.06.007.

15. Kristensen, C.A., Askenasy, N., Jain, R.K., and Koretsky, A.P. (1999). Creatine and cyclocreatine treatment of human colon adenocarcinoma xenografts: 31P and 1H magnetic resonance spectroscopic studies. Br. J. Cancer *79*, 278–285. https://doi.org/10.1038/sj.bjc.6690045.

16. Lagarde, D., and Kazak, L. (2021). Creatine promotes metastatic dissemination. Cell Metabol. *33*, 1065–1067. https://doi.org/10.1016/j.cmet.2021.05.012.

17. Lawler, J.M., Barnes, W.S., Wu, G., Song, W., and Demaree, S. (2002). Direct antioxidant properties of creatine. Biochem. Biophys. Res. Commun. *290*, 47–52. https://doi.org/10.1006/bbrc.2001.6164.

18. Miller, E.E., Evans, A.E., and Cohn, M. (1993). Inhibition of rate of tumor growth by creatine and cyclocreatine. Proc. Natl. Acad. Sci. USA *90*, 3304–3308. https://doi.org/10.1073/pnas.90.8.3304.

19. Tokarska-Schlattner, M., Epand, R.F., Meiler, F., Zandomeneghi, G., Neumann, D., Widmer, H.R., Meier, B.H., Epand, R.M., Saks, V., Wallimann, T., and Schlattner, U. (2012). Phosphocreatine interacts with phospholipids, affects membrane properties and exerts membrane-protective effects. PLoS One *7*, e43178. https://doi.org/10.1371/journal.pone.0043178.

20. Zucchi, R., Poddighe, R., Limbruno, U., Mariani, M., Ronca-Testoni, S., and Ronca, G. (1989). Protection of isolated rat heart from oxidative stress by exogenous creatine phosphate. J. Mol. Cell. Cardiol. *21*, 67–73. https://doi.org/10.1016/0022-2828(89)91494-6.

21. Barrett, A., Pellet-Many, C., Zachary, I.C., Evans, I.M., and Frankel, P. (2013). p130Cas: a key signalling node in health and disease. Cell. Signal. *25*, 766–777. https://doi.org/10.1016/j.cellsig.2012.12.019.

22. Centonze, G., Natalini, D., Salemme, V., Costamagna, A., Cabodi, S., and Defilippi, P. (2021). p130Cas/BCAR1 and p140Cap/SRCIN1 adaptors: the yin yang in breast cancer? Front. Cell Dev. Biol. *9*, 729093. https://doi.org/10.3389/fcell.2021.729093.

23. Defilippi, P., Di Stefano, P., and Cabodi, S. (2006). p130Cas: a versatile scaffold in signaling networks. Trends Cell Biol. *16*, 257–263. https://doi.org/10.1016/j.tcb.2006.03.003.

24. Tikhmyanova, N., Little, J.L., and Golemis, E.A. (2010). CAS proteins in normal and pathological cell growth control. Cell. Mol. Life Sci. *67*, 1025–1048. https://doi.org/10.1007/s00018-009-0213-1.

25. Aranda, S., Mas, G., and Di Croce, L. (2015). Regulation of gene transcription by Polycomb proteins. Sci. Adv. *1*, e1500737. https://doi.org/10.1126/sciadv.1500737.

26. Kouznetsova, V.L., Tchekanov, A., Li, X., Yan, X., and Tsigelny, I.F. (2019). Polycomb repressive 2 complex-Molecular mechanisms of function. Protein Sci. *28*, 1387–1399. https://doi.org/10.1002/pro.3647.

27. Torchy, M.P., Hamiche, A., and Klaholz, B.P. (2015). Structure and function insights into the NuRD chromatin remodeling complex. Cell. Mol. Life Sci. *72*, 2491–2507. https://doi.org/10.1007/s00018-015-1880-8.

28. Vizán, P., Beringer, M., Ballaré, C., and Di Croce, L. (2015). Role of PRC2-associated factors in stem cells and disease. FEBS J. *282*, 1723–1735. https://doi.org/10.1111/febs.13083.

29. Hassig, C.A., Fleischer, T.C., Billin, A.N., Schreiber, S.L., and Ayer, D.E. (1997). Histone deacetylase activity is required for full transcriptional repression by mSin3A. Cell *89*, 341–347. https://doi.org/10.1016/s0092-8674(00)80214-7.

30. Kitange, G.J., Mladek, A.C., Schroeder, M.A., Pokorny, J.C., Carlson, B.L., Zhang, Y., Nair, A.A., Lee, J.H., Yan, H., Decker, P.A., et al. (2016). Retinoblastoma binding protein 4 modulates temozolomide sensitivity in glioblastoma by regulating DNA repair proteins. Cell Rep. *14*, 2587–2598. https://doi.org/10.1016/j.celrep.2016.02.045.

31. Zhang, Q., Vo, N., and Goodman, R.H. (2000). Histone binding protein RbAp48 interacts with a complex of CREB binding protein and phosphorylated CREB. Mol. Cell Biol. *20*, 4970–4978. https://doi.org/10.1128/MCB.20.14.4970-4978.2000.

32. Zhang, Y., Iratni, R., Erdjument-Bromage, H., Tempst, P., and Reinberg, D. (1997). Histone deacetylases and SAP18, a novel polypeptide, are components of a human Sin3 complex. Cell *89*, 357–364. https://doi.org/10.1016/s0092-8674(00)80216-0.

33. Bonilla, B., Hengel, S.R., Grundy, M.K., and Bernstein, K.A. (2020). RAD51 gene family structure and function. Annu. Rev. Genet. *54*, 25–46. https://doi.org/10.1146/annurev-genet-021920-092410.

34. Wassing, I.E., and Esashi, F. (2021). RAD51: beyond the break. Semin. Cell Dev. Biol. *113*, 38–46. https://doi.org/10.1016/j.semcdb.2020.08.010.

35. Francescato, M.P., Cettolo, V., and di Prampero, P.E. (2008). Influence of phosphagen concentration on phosphocreatine breakdown kinetics. Data from human gastrocnemius muscle. J. Appl. Physiol. *105*, 158–164. https://doi.org/10.1152/japplphysiol.00007.2008.

36. Hetherington, H.P., Spencer, D.D., Vaughan, J.T., and Pan, J.W. (2001). Quantitative (31)P spectroscopic imaging of human brain at 4 Tesla: assessment of gray and white matter differences of phosphocreatine and ATP. Magn. Reson. Med. *45*, 46–52. https://doi.org/10.1002/1522-2594(200101)45:1<46::aid-mrm1008>3.0.co;2-n.

37. Kushmerick, M.J., Moerland, T.S., and Wiseman, R.W. (1992). Mammalian skeletal muscle fibers distinguished by contents of phosphocreatine, ATP, and Pi. Proc. Natl. Acad. Sci. USA *89*, 7521–7525. https://doi.org/10.1073/pnas.89.16.7521.

38. Gao, X., Wang, H., Yang, J.J., Liu, X., and Liu, Z.R. (2012). Pyruvate kinase M2 regulates gene transcription by acting as a protein kinase. Mol. Cell *45*, 598–609. https://doi.org/10.1016/j.molcel.2012.01.001.

39. Yang, W., Xia, Y., Hawke, D., Li, X., Liang, J., Xing, D., Aldape, K., Hunter, T., Alfred Yung, W.K., and Lu, Z. (2012). PKM2 phosphorylates histone H3 and promotes gene transcription and tumorigenesis. Cell *150*, 685–696. https://doi.org/10.1016/j.cell.2012.07.018.

40. Li, X., Jiang, Y., Meisenhelder, J., Yang, W., Hawke, D.H., Zheng, Y., Xia, Y., Aldape, K., He, J., Hunter, T., et al. (2016). Mitochondria-translocated PGK1 functions as a protein kinase to coordinate glycolysis and the TCA cycle in tumorigenesis. Mol. Cell *61*, 705–719. https://doi.org/10.1016/j.molcel.2016.02.009.

41. Xu, D., Li, X., Shao, F., Lv, G., Lv, H., Lee, J.H., Qian, X., Wang, Z., Xia, Y., Du, L., et al. (2019). The protein kinase activity of fructokinase A specifies the antioxidant responses of tumor cells by phosphorylating p62. Sci. Adv. *5*, eaav4570. https://doi.org/10.1126/sciadv.aav4570.

42. Xu, D., Wang, Z., Xia, Y., Shao, F., Xia, W., Wei, Y., Li, X., Qian, X., Lee, J.H., Du, L., et al. (2020). The gluconeogenic enzyme PCK1 phosphorylates INSIG1/2 for lipogenesis. Nature *580*, 530–535. https://doi.org/10.1038/s41586-020-2183-2.

43. Liu, R., Lee, J.H., Li, J., Yu, R., Tan, L., Xia, Y., Zheng, Y., Bian, X.L., Lorenzi, P.L., Chen, Q., and Lu, Z. (2021). Choline kinase alpha 2 acts as a protein kinase to promote lipolysis of lipid droplets. Mol. Cell *81*, 2722–2735.e9. https://doi.org/10.1016/j.molcel.2021.05.005.

44. Charoonpatrapong-Panyayong, K., Shah, R., Yang, J., Alvarez, M., Pavalko, F.M., Gerard-O'Riley, R., Robling, A.G., Templeton, E., and Bidwell, J.P. (2007). Nmp4/CIZ contributes to fluid shear stress induced MMP-13 gene induction in osteoblasts. J. Cell. Biochem. *102*, 1202–1213. https://doi.org/10.1002/jcb.21349.

45. Guo, A.K., Itahana, Y., Seshachalam, V.P., Chow, H.Y., Ghosh, S., and Itahana, K. (2021). Mutant TP53 interacts with BCAR1 to contribute to cancer cell invasion. Br. J. Cancer *124*, 299–312. https://doi.org/10.1038/s41416-020-01124-9.

46. Miyazaki, T., Zhao, Z., Ichihara, Y., Yoshino, D., Imamura, T., Sawada, K., Hayano, S., Kamioka, H., Mori, S., Hirata, H., et al. (2019). Mechanical regulation of bone homeostasis through p130Cas-mediated alleviation of NF-kappaB activity. Sci. Adv. *5*, eaau7802. https://doi.org/10.1126/sciadv.aau7802.

47. Li, L.Y., Guan, Y.D., Chen, X.S., Yang, J.M., and Cheng, Y. (2020). DNA repair pathways in cancer therapy and resistance. Front. Pharmacol. *11*, 629266. https://doi.org/10.3389/fphar.2020.629266.

48. Liu, Y.P., Zheng, C.C., Huang, Y.N., He, M.L., Xu, W.W., and Li, B. (2021). Molecular mechanisms of chemo- and radiotherapy resistance and the potential implications for cancer treatment. MedComm *2*, 315–340. https://doi.org/10.1002/mco2.55.

49. Laurini, E., Marson, D., Fermeglia, A., Aulic, S., Fermeglia, M., and Pricl, S. (2020). Role of Rad51 and DNA repair in cancer: a molecular perspective. Pharmacol. Ther. *208*, 107492. https://doi.org/10.1016/j.pharmthera.2020.107492.

50. Orhan, E., Velazquez, C., Tabet, I., Sardet, C., and Theillet, C. (2021). Regulation of RAD51 at the transcriptional and functional levels: what prospects for cancer therapy? Cancers *13*, 2930. https://doi.org/10.3390/cancers13122930.

51. Raderschall, E., Stout, K., Freier, S., Suckow, V., Schweiger, S., and Haaf, T. (2002). Elevated levels of Rad51 recombination protein in tumor cells. Cancer Res. *62*, 219–225.

52. Jiang, H., Khan, S., Wang, Y., Charron, G., He, B., Sebastian, C., Du, J., Kim, R., Ge, E., Mostoslavsky, R., et al. (2013). SIRT6 regulates TNF-alpha secretion through hydrolysis of long-chain fatty acyl lysine. Nature *496*, 110–113. https://doi.org/10.1038/nature12038.

53. Bong, S.M., Moon, J.H., Jang, E.H., Lee, K.S., and Chi, Y.M. (2008). Overexpression, purification, and preliminary X-ray crystallographic analysis of human brain-type creatine kinase. J. Microbiol. Biotechnol. *18*, 295–298.

STAR★METHODS

KEY RESOURCES TABLE

REAGENT or RESOURCE	SOURCE	IDENTIFIER
Antibodies		
BCAR1 antibody	Cell Signaling Technology	Cat#13846; RRID:AB_2798328
BCAR1 antibody	Santa Cruz Biotechnology	Cat#sc-20029; RRID:AB_628064
BCAR1 pY165 antibody	Cell Signaling Technology	Cat#4015; RRID:AB_2065459
BCAR1 pY249 antibody	Cell Signaling Technology	Cat#4014; RRID:AB_2243549
BCAR1 pY410 antibody	Cell Signaling Technology	Cat#4011; RRID:AB_2274823
BCAR1 pY751 antibody	Abcam	Cat#ab45486; RRID:AB_869932
BCAR1 pY327 antibody	This Study (made by PTM bio)	N/A
β-actin antibody	Thermo Fisher Scientific	Cat#MA1-140; RRID: AB_2536844
Flag-HRP	Sigma-Aldrich	Cat# F7425; RRID:AB_439687
RBBP4 antibody	Novus	Cat#NBP1-41201; RRID:AB_2238239
H4K16Ac antibody	Millipore	Cat#07-329; RRID:AB_310525
H4 antibody	Abcam	Cat#ab31830; RRID:AB_1209246
γH2AX antibody	Cell Signaling Technology	Cat#9718S; RRID:AB_2118009
H2AX antibody	Proteintech	Cat#10856-1-AP; RRID:AB_2114985
RAD51 antibody	Proteintech	Cat#14961-1-AP; RRID:AB_2177083
M2 Affinity gel	Sigma-Aldrich	Cat#A2220; RRID:AB_10063035
CKM antibody	Abcam	Cat#ab126244; RRID:AB_11127285
CKB antibody	Abcam	Cat#ab38211; RRID:AB_731614
pTyr antibody 4G10	Millipore	Cat#05-321; RRID:AB_309678
Myc tag antibody	Cell Signaling Technology	Cat#2040S; RRID:AB_2148465
Mouse monoclonal anti-Flag M2 antibody	Sigma-Aldrich	Cat#F1804; RRID:AB_262044
Goat anti-mouse IgG-HRP	Jackson ImmunoResearch Labs	Cat# 115-035-166; RRID:AB_2338511
Goat anti-rabbit IgG-HRP	Beyotime	Cat#A0208; RRID:AB_2892644
Alexa Fluor 790-anti-Rabbit	Jackson ImmunoResearch Labs	Cat#111-655-144; RRID:AB_2338086
Alexa Fluor 790-anti-Mouse	Jackson ImmunoResearch Labs	Cat#115-655-146; RRID:AB_2338944
Bacterial and virus strains		
DH5a	Tiangen	Cat# CB101-02
BL21(DE3) Chemically Competent Cell	TransGen	Cat# CD601
Chemicals, peptides, and recombinant proteins		
Anti-Flag Affinity Gel	Bimake	Cat#B23102
Anti-Myc magnetic beads	Bimake	Cat#B26301
Anti-Phosphotyrosine Antibody, clone 4G10, agarose conjugate	Millipore	Cat#16-101
Amicon ultra 0.5mL 10K	Millipore	Cat#UFC5010BK
Dialysis membrane	Sangon Biotech	Cat#F132590
EZ Trans	Life iLab Bio	Cat#C4058L1092
Nhe I	New England Biolabs	Cat#R3131S
EcoR I	New England Biolabs	Cat#R3101S
BamHI-HF	New England Biolabs	Cat#R3136L
TGF-β	Absin	Cat#abs04204

(*Continued on next page*)

Continued

REAGENT or RESOURCE	SOURCE	IDENTIFIER
etopside (Cas No.33419-42-0)	tansoole	Cat#01158693
TRIzol reagent	Thermo Fisher Scientific	Cat#15596-026
cOmplete™, Mini, EDTA-free Protease Inhibitor Cocktail (protease inhibitor cocktail)	Roche	Cat#4693159001
PhosSTOP (phosphatase inhibitors)	Roche	Cat#4906845001
His-CKB WT	This study	N/A
His-CKB R292Q	This study	N/A
His-CKB R292K	This study	N/A
His-CKB C283S	This study	N/A
dialyzed FBS	Thermo Fisher Scientific	Cat#30067334
pervanadate	This study	N/A
Critical commercial assays		
Hieff Clone® Plus One Step Cloning Kit	Yeason	Cat#10911ES20
CometAssay® Kit 50 Samples (25X2 well slides)	Trevigen	Cat#4250-050-K
PrimeScript RT master Mix qPCR	Takara, Japan	Cat#RR036Q
TB Green Premix Ex TaqII (Takara, Japan)	Takara, Japan	Cat#RR820A
QIAquick PCR Purification Kit	Qiagen	Cat#28104
SimpleChIP® Plus Sonication Chromatin IP Kit	CST	Cat#56383
Deposited data		
Proteomics data	This Study	IProx: PXD041365 (https://www.iprox.cn)
Experimental models: Cell lines		
293T CKB/CKM DKD cells	This study	N/A
293T CKB KD cells	This study	N/A
MCF7 BCAR1-WT OE cells	This study	N/A
MCF7 BCAR1-WT YF cells	This study	N/A
MCF7 CKB KD cells	This study	N/A
MCF7 BCAR1 KD cells	This study	N/A
MCF7 GFP KD cells	This study	N/A
Oligonucleotides		
Primers used for molecular cloning of expression vectors, see Table S1	This study	N/A
Primers for qPCR analyses, see Table S2	This study	N/A
Primers for ChIP qPCR analyses, see Table S3	This study	N/A
Targeting sequences for shRNAs, see Table S4	This study	N/A
Recombinant DNA		
psPAX2	Hu Junhao (Shanghai Institute of Organic Chemistry)	N/A
pMD2.G	Hu Junhao (Shanghai Institute of Organic Chemistry)	N/A
pLKO.1-shGFP	Junying Yuan (Shanghai Institute of Organic Chemistry)	N/A
pLKO.1	Junying Yuan (Shanghai Institute of Organic Chemistry)	N/A
pSIN-CKB-Myc	This Study	N/A

(*Continued on next page*)

Continued

REAGENT or RESOURCE	SOURCE	IDENTIFIER
pSIN-CKB-Myc-C283S	This Study	N/A
pSIN-CKB-Myc-R292K	This Study	N/A
pSIN-CKB-Myc-R292Q	This Study	N/A
pET-28a-His-CKB	This Study	N/A
pET-28a-His-CKB-C283S	This Study	N/A
pET-28a-His-CKB-R292K	This Study	N/A
pET-28a-His-CKB-R292Q	This Study	N/A
pSIN-BCAR1-Flag-Y12F	This Study	N/A
pSIN-BCAR1-Flag-Y67F	This Study	N/A
pSIN-BCAR1-Flag-Y99F	This Study	N/A
pSIN-BCAR1-Flag-Y107F	This Study	N/A
pSIN-BCAR1-Flag-Y115F	This Study	N/A
pSIN-BCAR1-Flag-Y128F	This Study	N/A
pSIN-BCAR1-Flag-Y165F	This Study	N/A
pSIN-BCAR1-Flag-Y179F	This Study	N/A
pSIN-BCAR1-Flag-Y192F	This Study	N/A
pSIN-BCAR1-Flag-Y222F/Y224F	This Study	N/A
pSIN-BCAR1-Flag-Y234F	This Study	N/A
pSIN-BCAR1-Flag-Y249F	This Study	N/A
pSIN-BCAR1-Flag-Y262F	This Study	N/A
pSIN-BCAR1-Flag-Y267F	This Study	N/A
pSIN-BCAR1-Flag-Y287F	This Study	N/A
pSIN-BCAR1-Flag-Y306F	This Study	N/A
pSIN-BCAR1-Flag-Y362F	This Study	N/A
pSIN-BCAR1-Flag-Y372F	This Study	N/A
pSIN-BCAR1-Flag-Y387F	This Study	N/A
pSIN-BCAR1-Flag	This Study	N/A
pSIN-BCAR1-Flag-Y327F	This Study	N/A
pSIN-BCAR1-Flag-Y327E	This Study	N/A
pSIN-BCAR1-Flag-SD-18F	This Study	N/A
pSIN-BCAR1-Flag-S134A	This Study	N/A
pSIN-N-Flag-BCAR1	This Study	N/A
pSIN-N-Flag-BCAR1(1-453)	This Study	N/A
pSIN-N-Flag-BCAR1(1-634)	This Study	N/A
pSIN-N-Flag-BCAR1(1-677)	This Study	N/A
pSIN-N-Flag-BCAR1(1-734)	This Study	N/A
pSIN-N-Flag-BCAR1(454-870)	This Study	N/A
pSIN-N-Flag-BCAR1(635-870)	This Study	N/A
pSIN-N-Flag-BCAR1(668-870)	This Study	N/A
pSIN-RBBP4-myc	This Study	N/A
shRNA-resistant BCAR-Flag WT in pSIN vector (rBCAR1 WT)	This Study	N/A
shRNA-resistant BCAR-Flag Y327F in pSIN vector (rBCAR1 YF)	This Study	N/A
pSIN-GFP-Flag	This Study	N/A

(*Continued on next page*)

Continued

REAGENT or RESOURCE	SOURCE	IDENTIFIER
pSIN-N-Flag-BCAR1(1-734)	This Study	N/A
pSIN-N-Flag-BCAR1(454-870)	This Study	N/A
pSIN-N-Flag-BCAR1(635-870)	This Study	N/A
pSIN-N-Flag-BCAR1(668-870)	This Study	N/A
pSIN-RBBP4-myc	This Study	N/A
shRNA-resistant BCAR-Flag WT in pSIN vector (rBCAR1 WT)	This Study	N/A
shRNA-resistant BCAR-Flag Y327F in pSIN vector (rBCAR1 YF)	This Study	N/A
pSIN-GFP-Flag	This Study	N/A
pSIN-N-Flag-BCAR1(635-870)	This Study	N/A
pSIN-N-Flag-BCAR1(668-870)	This Study	N/A
pSIN-RBBP4-myc	This Study	N/A
shRNA-resistant BCAR-Flag WT in pSIN vector (rBCAR1 WT)	This Study	N/A
shRNA-resistant BCAR-Flag Y327F in pSIN vector (rBCAR1 YF)	This Study	N/A
pSIN-GFP-Flag	This Study	N/A
Software and algorithms		
GraphPad Prism 8.0	GraphPad Software	https://www.graphpad.com/
MaxQuant software (version 1.5.3.30)	Max Planck Institute of Biochemistry	https://www.biochem.mpg.de/6304115/maxquant
ImageJ	NIH	https://imagej.nih.gov/ij/
Image Studio (version 5.2.5)	LI-COR Imaging Systems	https://www.licor.com/bio/image-studio/resources

RESOURCE AVAILABILITY

Lead contact

Further information and requests for resources and reagents should be directed to and will be fulfilled by the corresponding author, Dr. Hong Jiang (hongjiang@sioc.ac.cn).

Materials availability

Reagents generated in this study are available on request with a completed Materials Transfer Agreement.

Data and code availability

- The proteomics data is deposited in the public database iProX (https://www.iprox.cn) and the accession number iProX: PXD041365 is provided in the key resources table. We also supplied the processed data of proteome as the Data S1 and S2.
- No code was developed for this study.
- Any additional information required to reanalyze the data reported in this paper is available from the lead contact upon request.

EXPERIMENTAL MODEL AND SUBJECT DETAILS

Cell lines

HEK 293T, MCF7, MCF7 CKB KD cells were maintained in DMEM supplemented with 10% FBS and 1% penicillin-streptomycin in a 5% CO_2 incubator at 37°C. 293T CKB/CKM DKD cells were maintained in DMEM supplemented with 10% dialyzed FBS and 1% penicillin-streptomycin in a 5% CO_2 incubator at 37°C. All cell lines had been tested negative for mycoplasma contamination.

Generation of stable KD cells

MCF-7 CKB stable KD cells (shCKB#1, shCKB#2), BCAR1 stable KD cells (shBCAR1#1, shBCAR1#2), or RBBP4 stable KD cells (shRBBP4#1, shRBBP4#2) were generated by shRNAs (Table S4) in pLKO.1 vector targeting human CKB or BCAR1, respectively. 293T CKB stable KD cells were generated by shRNA in pLKO.1 vector targeting human CKB (shCKB#2) (Table S4). 293T CKB/CKM stable DKD cells were generated by shRNAs in pLKO.1 vector targeting human CKB (shCKB#2) and CKM (shCKM#1) (Table S4), respectively. HEK 293T cells were co-transfected with lentiviral plasmid DNA, pMD2.G and psPAX2 for 48 h. Then culture medium containing lentivirus was collected and cleared for 10 min at 3 000 *g* at room temperature. Target cells were infected by virus for two days and further selected with puromycin or blasticidin for 3 generations. Selected cells were verified by WB and then used for further experiments.

Generation of stable overexpression cells

Human BCAR1-Flag WT/Y327F/Y327E stable overexpression cells were generated by pSIN lentiviral vector (engineered from pSIN-EF2-OCT4 vector).[52] cDNA encoding human BCAR1 WT was cloned into a pSIN lentiviral vector using Hieff Clone Plus One Step Cloning Kit and corresponding primers (Table S1 primers). BCAR1-Flag Y327F and Y327E were generated by overlap PCR and then cloned into pSIN vector. After 293Tcells were co-transfected with lentiviral plasmid, psPAX2 and pMD2.G, culture medium was collected to infect target cells for two days. Then infected cells were selected with puromycin for 3 generations. Selected cells were verified by WB and then used for further experiments.

METHOD DETAILS

Plasmid construction

Plasmids used in this study are summarized in Table S1. Plasmids of Flag-BCAR1 full length/truncations, BCAR1-Flag WT/mutants and shRNA-resistant BCAR-Flag WT/Y327F (targeting shBCAR1#1) used human full-length BCAR1 as the template. Plasmids of CKB-Myc WT/mutants and His-CKB WT/mutants used human full-length CKB as the template. RBBP4 plasmid used human full-length RBBP4 as the template. Target cDNA was cloned into a pSIN lentiviral vector or pET28a vector using Hieff Clone Plus One Step Cloning Kit and corresponding primers (Table S1 primers). All mutations were generated by PCR-mediated site-directed mutagenesis on corresponding plasmids (Table S1 primers).

Dialyzed cell lysates for *in vitro* phosphorylation assay

293T CKB KD cells or CKB/CKM DKD cells (70% confluency, cultured with dialyzed FBS) were lysed with 1% NP-40 buffer (25 mM Tris-HCl, pH 7.4, 150 mM NaCl, 1% protease inhibitor cocktail, 1% NP-40) at 4 °C for 30 min. After centrifugation at 20 000 *g* for 30 min at 4 °C, the supernatant was collected and dialyzed 3 times in dialysis Buffer (25 mM Tris-HCl, pH 7.4, 150 mM NaCl, 1% protease inhibitor cocktail, 10% Glycerol) with each time for 3 h at 4 °C.

Protein purification of N-His-CKB WT, R292Q, R292K and C283S

To purify proteins of N-His-CKB WT and mutants, target genes were cloned into pET-28a vector (Table S1 primers). The recombinant proteins were expressed in BL21(DE3) *E. coli* strain and purified according to the reference 53. Briefly, the cells were grown at 37 °C and induced by 0.5 mM IPTG when OD600 reached 0.5. After additional growth at 37 °C for 5 h, cells were collected and lysed in Buffer A (20 mM HEPES, 300 mM NaCl, 10% Glycerol, pH 7.5) by high pressure cell disrupter. The recombinant protein was purified by a HisTrap column (Cytiva, 1 x 5 ml, Cat#17524801) using linear gradient of Buffer B (20 mM HEPES, 300 mM NaCl, 10% Glycerol, 500 mM imidazole, pH 7.5) in Buffer A.

Protein purification of BCAR1-Flag WT and mutants

293T CKB/CKM DKD cells were transfected with pSIN-BCAR1–Flag WT or mutants for 24 h and then lysed in 1% NP-40 buffer (25 mM Tris-HCl, pH 7.4, 150 mM NaCl, 1% protease inhibitor cocktail, 1% NP-40) at 4°C. After centrifugation at 20 000 *g* for 30 min at 4 °C, the supernatant was collected. Target proteins were enriched by immunoprecipitation using Flag-beads at 4°C and eluted by 0.15 mg/ml 3×Flag peptide in TBS overnight.

In vitro phosphorylation assay

For assays for cell lysates: in 50 μL reaction buffer, dialyzed cell lysate (2 μg/μL) was treated with bacterially purified His-CKB (0.4 or 2 μg/μL), PCr (1 mM) and $MgCl_2$ (5 mM) with or without cyclo-Cr (2 mM) at 37 °C for

1 h. For assays for purified BCAR1 proteins: in 20 μL reaction buffer, BCAR1-Flag (2 μg/μL, WT or mutants purified from 293T CKB/CKM DKD cells) was treated with bacterially purified His-CKB (1 μg/μL), PCr (1 or 5 mM) and $MgCl_2$ (5 mM) at 37 °C for 1 h. The control reactions were performed without His-CKB, PCr or $MgCl_2$. Reaction buffer: 50 mM HEPES, pH 7.5, 150 mM NaCl. The reactions were terminated by addition of 2×protein loading dye and then subjected to pTyr IP, SDS-PAGE or WB analyses.

Generation and validation of BCAR1 pY327 antibody

BCAR1 pY327 antibody was ordered from PTMBIO (HangZhou, ZheJiang, China) (http://www.ptm-biolab.com.cn/index.html). To validate BCAR1 pY327 antibody by Dot Blot, various amounts of the immunogen peptide CLREET-(phospho)Y-DVPPAF and negative control peptide CLREETYDVPPAF (without phosphorylation) on the nitrocellulose filter membrane were applied (Figure S3A). To validate BCAR1 pY327 antibody for proteins by western blot, pervanadate-treated 293T and MCF-7 cell lysates with overexpression of BCAR1-Flag WT, Y327F and Y327E were used (Figure S3B).

Western blotting

Cells were lysed in 1% NP-40 buffer (50 mM Tris-HCl, pH 7.4,150 mM NaCl, 10% glycerol, 1% NP-40 and 1% protease inhibitor cocktail) or RIPA buffer (50 mM Tris-HCl, pH 7.4,150 mM NaCl, 1% Triton X-100, 1% deoxycholate, 0.1% SDS, 10% glycerol and 1% protease inhibitor cocktail). After centrifugation at 20 000 g for 30 min at 4°C, the supernatant was collected for SDS-PAGE and WB analyses. The western blot images were (1) captured and analyzed by chemiluminescence system (Fusion FX, VILBER, France); (2) incubated for 1 h with rocking in Li-Cor secondary antibodies and captured by Li-Cor Odyssey CLX. The optical density of immunoblotting bands was quantified using ImageJ or Image Studio program and was normalized to the corresponding controls.

Co-immunoprecipitation and immunoprecipitation

After cells were transiently transfected with expressing plasmids for 36 h, cells were harvested and lysed with 1% NP-40 buffer (25 mM Tris-HCl, pH 7.4, 150 mM NaCl, 1% protease inhibitor cocktail, 1% NP-40) at 4°C. After centrifugation at 15 000 g for 15 min at 4°C, the supernatant was collected, diluted 5 times with washing buffer (50 mM Tris-HCl, pH 7.4, 150 mM NaCl, 10% glycerol and 1% protease inhibitor cocktail) and then incubated with a control IgG or specific antibody for 2-4 hrs. Target proteins were enriched by protein A/G beads overnight. The immunoprecipitates were washed for 3 times by washing buffer and subjected to immunoblot analysis. Flag beads were used in Flag-tagged protein immunoprecipitation. For denaturing IP, samples were precipitated using methanol/chloroform and resolubilized in 1% SDS buffer (25 mM Tris-HCl, pH 7.4, 150 mM NaCl, 1% SDS) with sonication. Then samples were diluted to 0.1% SDS by adding 0.2% NP-40 buffer (25 mM Tris-HCl, pH 7.4, 150 mM NaCl, 1% protease inhibitor cocktail, 0.2% NP-40) for immunoprecipitation.

Enrichment of phosphotyrosine proteins for phosphoproteomics

In 2 mL reaction buffer, dialyzed 293T CKB KD cell lysate (2 μg/μL) was treated with bacterially purified His-CKB (0.4 μg/μL), PCr (1 mM) and $MgCl_2$ (5 mM) at 37 °C for 1 h (sample S1). The control reactions were performed without His-CKB (sample S2), PCr (sample S3) or both (sample S4). All the reactions were repeated 3 times. Samples were precipitated using methanol/chloroform and resolubilized in 1% SDS buffer (25 mM Tris-HCl, pH 7.4, 150 mM NaCl, 1% SDS) with sonication. Then samples were diluted to 0.1% SDS by adding 0.2% NP-40 buffer (25 mM Tris-HCl, pH 7.4, 150 mM NaCl, 1% protease inhibitor cocktail, 0.2% NP-40) for immunoprecipitation using pTyr-beads (Millipore) to enrich phosphotyrosine proteins for on-beads digestion.

IP-MS of BCAR1-Flag WT and Y327F from 293T cells

After transfected with BCAR1-Flag WT or Y327F plasmid (6 μg plasmid with 18 μl PEI) for 24 h, 293T cells were harvested and lysed in 1%NP-40 buffer (25 mM Tris-HCl, pH 7.4, 150 mM NaCl, 1% protease inhibitor cocktail, 1% NP-40). The experiments were repeated 5 times for both BCAR1-Flag WT and Y327. After normalization of BCAR1-Flag WT and Y327F protein amounts in the samples, Flag IP was executed to enrich BCAR1-Flag WT or Y327F with their interacting proteins for on-beads digestion.

On-beads digestion

Beads were suspended in 500 μL of 6 M Urea in PBS and treated with 10 mM Tris(2-carboxyethyl)-phosphine for 30 min at room temperature followed by the treatment of 25 mM iodoacetamide for 30 min at room temperature. The supernatant was collected and the urea concentration was diluted to 2 M with PBS. Then the solution was treated with 1 mM $CaCl_2$ and 2 μg trypsin for digestion at 37°C for 12 h. Digested peptides were enriched by C18 tips for LC-MS/MS detection.

LC-MS/MS analysis

The peptide mixtures were analyzed using an on-line EASY-nL-LC 1000 coupled with an Orbitrap Fusion mass spectrometer. The sample was loaded directly onto a 15-cm home-made capillary column (C18-AQ, 1.9 mm, Dr. Maisch, 100 mm I.D.) at a flow rate of 300 nl/min. Mobile phase A consisted of 0.1% formic acid, 2% acetonitrile and 98% H_2O and mobile phase B consisted of 0.1% formic acid, 2% H_2O and 98% acetonitrile.

For IP-MS analysis, data were acquired in a data-dependent mode with one full MS1 scan in the Orbitrap (m/z: 200–1800; resolution: 120 000; AGC target value: 400 000 and maximal injection time: 50 ms), followed by MS2 scan in the in the Orbitrap (32% normalized collision energy; resolution: 30 000; AGC target value: 10 000; maximal injection time: 100 ms).

For phosphoproteomic analysis, data were acquired in a data-dependent mode with one full MS1 scan in the Orbitrap (m/z: 350–1500; resolution: 120 000; AGC target value: 1 000 000 and maximal injection time: 20 ms), followed by MS2 scan in the in the Orbitrap (32% normalized collision energy; resolution: 30 000; AGC target value: 100 000; maximal injection time: 45 ms).

MS data analysis

MS/MS raw spectra were processed using MaxQuant software (version 1.5.3.30). The human protein sequence database containing 20410 sequence entries in the Swiss-Prot database downloaded on October 12, 2018 was used for database search. Trypsin was set as the enzyme, and the maximum missed cleavage was set to 2. The first-search peptide mass tolerance and main-search peptide tolerance were set to 20 and 4.5 ppm. The MS/MS match tolerance was set to 0.5 Da for ITMS and 20 ppm for FTMS. A fixed carbamidomethyl modification of cysteine and variable modifications including oxidation on methionine and phosphorylation on tyrosine were set. "Match between runs" was applied, and the match time window was set to within 2 min. The false discovery rate (FDR) was controlled with a decoy database and set to no more than 1%. For IP-MS analysis, protein hits are required to be at least detected in 3 out of 5 repeat samples of either BCAR1-Flag WT or Y327F. Undetected MS intensities are set as 500000 for calculation. Proteins with "ratio BCAR1 WT/Y327F > 5, p value < 0.01" or "ratio BCAR1 WT/Y327F < 0.20, p value < 0.01" are categorized in "UP" or "Down" group, respectively. For phosphoproteomic analysis, protein hits are required to be detected in all 3 S1 repeat samples. Undetected MS intensities are set as 500000 for calculation. Candidate substrates of CKB and PCr are identified with the cutoff ratios (S1/S2 > 3, S1/S3 > 10, and S1/S4 > 10).

RNA Preparation and RT-PCR

mRNA levels of RAD51 were measured in: (1) MCF-7 BCAR1 stable KD cells infected with rBCAR1-Flag WT/Y327F or GFP-Flag lentivirus for 3 days; and (2) MCF-7 CKB stable KD cells (shCKB#1, shCKB#2) and GFP stable KD cells (shGFP). Cells were cultured with 5 ng/ml TGF-β for 24 h before examination. Total RNA was extracted using the TRIzol reagent (Thermo Fisher Scientific, USA) according to the manufacturer's protocol. RNA was transcribed into cDNA using the PrimeScript RT master Mix qPCR (Takara, Japan). Real-time PCR was performed using the TB Green Premix Ex TaqII (Takara, Japan). Gene expression levels were calculated based on the $2^{-\Delta\Delta CT}$ relative quantification methods. The primers used in this study are listed in Table S2.

ChIP-qPCR assay and ChIP Re-ChIP assay

The ChIP-qPCR assay was performed according to the manufacturer's instructions (CST SimpleChIP) for (1) MCF-7 BCAR1 stable KD cells infected with rBCAR1-Flag WT/Y327F or GFP-Flag lentivirus for 3 days; (2) MCF-7 CKB stable KD cells (shCKB#1, shCKB#2) and GFP stable KD cells (shGFP); and (3) MCF-7 RBBP4 stable KD cells (shRBBP4#1, shRBBP4#2) and GFP stable KD cells (shGFP) overexpressing BCAR1-Flag

WT/Y327F or GFP-Flag. Briefly, after treated with 5 ng/ml TGF-β for 24 h, cells were fixed with 1% formaldehyde at room temperature for 10 min and quenched with 1×Glycine buffer for 5 min. Then cells were lysed with cell lysis buffer, and cell nuclei were collected and resuspended in Nuclear Lysis Buffer. Bioruptor Pico (Diagenode) or Scientz-IID Ultrasonic Cell Crusher were used to shear DNA to 200-1000bp fragments. RBBP4 antibody, H4K16Ac antibody and Flag antibody were used for ChIP. Enriched DNA fragments from ChIP samples were eluted with CHIP Elution Buffer and extracted by Qiagen PCR cleanup kit. qPCR was performed using *RAD51* promoter region primers (Table S3).

The ChIP re-ChIP experiments were performed according to the manufacturer's instructions (CST SimpleChIP) for 293T cells co-transfected with RBBP4-Myc and BCAR1-Flag WT/Y327F. Briefly, cells were fixed with 1% formaldehyde at room temperature for 10 min and quenched with 1×Glycine buffer for 5 min. Then cells were lysed with cell lysis buffer, and cell nuclei were collected and resuspended in Nuclear Lysis Buffer. Bioruptor Pico (Diagenode) was used to shear DNA to 200-1000bp fragments. First ChIP was executed with Myc beads (Bimake). Enriched DNA fragments were eluted with CHIP Elution Buffer for second ChIP with Flag beads (Bimake). The final enriched DNA fragments were eluted with CHIP Elution Buffer and extracted by Qiagen PCR cleanup kit. qPCR was performed using *RAD51* and *MGMT* promoter region primers (Table S3).

Neutral comet assay

Comet assays were carried out for (1) MCF-7 cells stably overexpressing BCAR1-Flag WT/Y327F/Y327E or empty vector; (2) MCF-7 BCAR1 stable KD cells infected with rBCAR1-Flag WT/Y327F/Y327E or empty vector lentivirus for 3 days; (3) MCF-7 CKB stable KD cells (shCKB#1, shCKB#2) and GFP stable KD cells (shGFP); (4) MCF-7 RBBP4 stable KD cells (shRBBP4#1, shRBBP4#2) and GFP stable KD cells (shGFP); and (5) MCF-7 CKB or RBBP4 stable KD cells infected with BCAR1-Flag WT/Y327F/Y327E or empty vector lentivirus for 3 days. After treatment of 20 μM etoposide or DMSO for 4 h, cells were harvested and adjusted to the density of 10^7 cells/l. Then cell suspension was mixed with LMAgarose (Trevigen, Gaithersburg, MD) at the ratio of 1:10 (v/v) at 37°C. 50 μL cell suspension was transferred onto a CometSlide and the slide was placed at 4°C for 10 min. After submerged in Lysis Solution and incubated for 2 h, the slide was subjected to electrophoresis at 25 V, 30 mA for 30 min. Then the slide was stained with GelRed and analyzed with a fluorescence microscope. Tail moment was determined by OpenComet software.

QUANTIFICATION AND STATISTICAL ANALYSIS

Experimental results were presented as mean ±SD. A two-tailed unpaired t test was used for the comparison between two experimental groups. GraphPad Prism (Version 8.0.1) was used for statistical calculations. For comparisons of multiple groups, One-way ANOVA was used. A log-rank test was performed for survival analysis.